

Activity and Kinematics of Ultracool Dwarfs Including An Amazing Flare Observation

Sarah J. Schmidt,^{1,2,3,4} Kelle L. Cruz,^{1,4,5} Bethany J. Bongiorno,^{1,2} James Liebert,^{4,6} and I. Neill Reid^{4,7}

sjschmidt@astro.washington.edu

ABSTRACT

We present the activity and kinematics of a representative volume-limited (20 pc) sample of 152 late-M and L dwarfs (M7–L8) photometrically selected from the Two Micron All-Sky Survey (2MASS). Using new proper motion measurements and spectrophotometric distance estimates, we calculate tangential velocities. The sample has a mean tangential velocity of $\langle V_{tan} \rangle = 31.5 \text{ km s}^{-1}$, a velocity dispersion of $\sigma_{tan} = 20.7 \text{ km s}^{-1}$, and a maximum tangential velocity of $V_{tan} = 138.8 \text{ km s}^{-1}$. These kinematic results are in excellent agreement with previous studies of ultracool dwarfs in the local solar neighborhood. $H\alpha$ emission, an indicator of chromospheric activity, was detected in 63 of 81 late-M dwarfs and 16 of 69 L dwarfs examined. We find a lack of correlation between activity strength, measured by $\log(F_{H\alpha}/F_{bol})$, and V_{tan} , though velocity distributions suggest that the active dwarfs in our sample are slightly younger than the inactive dwarfs. Consistent with previous studies of activity in ultracool dwarfs, we find that the fraction of $H\alpha$ emitting objects per spectral type peaks at spectral type M7 and declines through mid-L dwarfs. Activity strength is similarly correlated with spectral type for spectral types later than M7. Eleven dwarfs out of 150 show evidence of variability, ranging from small fluctuations to large flare events. We estimate a flare cycle of $\sim 5\%$ for late-M dwarfs and $\sim 2\%$ for L dwarfs. Observations of strong, variable activity on the L1 dwarf 2MASS J10224821+5825453 and an amazing flare event on the the M7 dwarf 2MASS J1028404–143843 are discussed.

Subject headings: Galaxy: stellar content — solar neighborhood — stars: activity — stars: flare — stars: late-type stars: low-mass, brown dwarfs — stars: individual (2MASS J10224821+5825453, 2MASS J1028404–143843)

¹Department of Astrophysics, American Museum of Natural History, New York, NY

²Department of Physics & Astronomy, Barnard College, Columbia University, New York, NY

³Department of Astronomy, University of Washington, Seattle, WA

⁴Visiting astronomer, Kitt Peak National Observatory and/or Cerro Tololo Inter-American Observatory, National Optical Astronomy Observatories, which are operated by the Association of Universities for Research in Astronomy, under contract with the National Science Foundation.

⁵NSF Astronomy and Astrophysics Postdoctoral Fellow

⁶Department of Astronomy and Steward Observatory, University of Arizona, Tucson, AZ

⁷Space Telescope Science Institute, Baltimore, MD

1. Introduction

The identification of large numbers of early-to-mid M dwarfs has enabled studies focused on their activity and kinematics (Reid et al. 1995; Hawley et al. 1996; Bochanski et al. 2005) and recent work has extended these investigations to late-M and early-L dwarfs (Gizis et al. 2000; West et al. 2004, 2006) but faint magnitudes and small numbers have prevented a thorough study of the activity and kinematics of L dwarfs. In order to fill that gap, we analyze a sample of ultracool dwarfs (spectral types M7–L8) photometrically selected from the the Two Micron All Sky Survey (Skrutskie et al. 2006, 2MASS). The Two

Micron Proper Motion sample (2MUPM sample) is a combination of a complete sample selected from the 2MASS Second Incremental Data Release (Cruz et al. 2003, 2006, in press) and the spectroscopically confirmed portion of a sample constructed from the All-Sky Data Release (Reid et al. 2007, in prep). This comprehensive survey allows us to investigate the activity and kinematics of cooler, fainter dwarfs in a sample with well documented properties and uncertainties.

We measured proper motions using the images provided by the Digitized Sky Survey (hereafter DSS), which combines data from the Palomar Observatory Sky Survey (Reid et al. 1991, POSS) and the UK Schmidt survey (Morgan 1995). Together, DSS images and 2MASS coordinates and images have enabled long baseline proper motion measurements for all but the 12 faintest objects, and the inclusion of new data has allowed us to obtain proper motions for all but seven dwarfs. We combine our proper motions with spectrophotometric distance estimates to obtain tangential velocities for our sample of 152 ultracool dwarfs. Kinematics allow us to investigate the age distribution of our sample; the ages of L dwarfs are of particular interest because the spectral class encompasses both stellar and substellar objects (Burrows et al. 2001).

Kinematics can also be combined with H α measurements to test the validity of an age activity relationship for ultracool dwarfs. The power law relationship between activity and age in main sequence stars (Skumanich 1972; Soderblom et al. 1991) breaks down during the M spectral class (Silvestri et al. 2005; Gizis et al. 2000). Kinematic studies show that active M dwarfs tend to be younger than inactive M dwarfs, but it is unknown whether this is due to a sharp cut-off in activity as dwarfs age, or a steady decline (West et al. 2004, 2006).

Activity is more closely related to spectral type in ultracool dwarfs. For M1 to M7 dwarfs, the fraction of active objects increases with later spectral type while the strength of H α emission remains relatively constant, though with scatter (Hawley et al. 1996; West et al. 2004; Bochanski et al. 2005). For M7 to late-L dwarfs, H α emission becomes increasingly less common with later spectral type as the activity strength de-

creases (Gizis et al. 2000; West et al. 2004). There is evidence that this relationship may extend into the T spectral class (Burgasser et al. 2002)

The mechanisms producing flare events and strong H α emission in ultracool dwarfs are not completely understood. Current estimates of the M dwarfs flare flare rate are approximately 7% (Gizis et al. 2000; Reid et al. 1999). Only a few L dwarfs have been observed with strong H α emission and little is known about their flare properties (Liebert et al. 1999, 2003; Hall 2002).

We present proper motions and H α measurements of a sample of 152 ultracool dwarfs with spectral types from M7–L8. In § 2, we discuss the completeness and properties of our sample. Details of proper motion measurements and the examination of spectral features are contained in § 3. We discuss the kinematics in § 4 and in § 5 we examine the activity properties of the sample and investigate possible age relations. Variability is discussed in § 6, including an strong variability on the L1 dwarf 2MASS J10224821+5825453 and an amazing flare on the M7 dwarf 2MASS J1028404–143843.

2. The Sample

To construct the 2MUPM sample of late-M and L dwarfs discussed in this paper, we have combined objects selected from both the 2MASS Second Incremental Data Release and the All-Sky Data Release. The dwarfs selected out of the second release are from Cruz et al. (2003, hereafter Paper V) and Cruz et al. (2006, in press, hereafter Paper IX). The dwarfs selected out of the all-sky release are from Reid et al. (2007, in prep, hereafter Paper X). Those papers describe how extensive follow up spectroscopy was obtained for candidate objects from both samples. Spectroscopy has been completed for the objects selected from the second release, but more observations are needed to finish confirmation and spectral typing for the objects selected from the all-sky release.

Though we summarize here, more details on sample selection, spectroscopy, spectral types, and spectrophotometric distance estimates can be found in Papers V, IX, and X. Spectral types were assigned by visual comparison of each spectra to spectral standards. There is an uncertainty of ± 0.5 spectral subtype for most dwarfs, and

whole number types are favored over half types. Spectrophotometric distance estimates were derived from a relation between spectral type and absolute J magnitude.

The subset of the sample selected from the 2MASS second release is complete for spectral types M9–L6 within a distance limit of 20 pc, but we include types M7–L8 in the 2MUPM sample. The color selection ($J - K > 1$) excludes the bluest M7 and M8 dwarfs, and magnitude limits exclude the most distant L7 and L8 dwarfs. Despite this incompleteness, there is no evidence that the near infrared selection criteria used to create the sample is correlated with activity or kinematics. The 2MASS second release sample comprises only 35 L dwarfs within 20 parsecs. In order to increase the sample size, we have included spectroscopically classified dwarfs within 20 pc from the all-sky sample, which adds 37 L dwarfs to the 2MUPM sample. As described above, we have not yet completed observations of the faintest objects from latter dataset; however, those omissions should not bias the activity or kinematic distributions of the sample as a whole.

The sample selected from the 2MASS second release is the basis of the luminosity function of ultracool dwarfs. Excepting a small number of dwarfs excluded because we could not measure proper motions, that portion of the 2MUPM sample has the same completeness discussed in Paper IX. While observations of the sample selected from the 2MASS all-sky release have not been completed, it was created with similar selection criteria. Figure 1 shows the number of objects per spectral type included from the second release selection and the all-sky selection. Excepting M7 dwarfs, which were purposely excluded from the all-sky selected sample, a K-S test indicates no difference between the two spectral type distributions at the 90% significance level.

The 2MASS-selected 20 parsec sample is currently composed of 170 dwarfs with spectral types from M7 to L8. The 2MUPM sample includes 11 multiple systems without resolved spectroscopy. The spectral types of both the primary and the secondary in these systems are estimated to be between M7 and L8. Because the lack of resolved spectroscopy does not allow us to check each object for $H\alpha$ emission, we consider the system as a single object with the spectral type of the pri-

mary. This excludes 11 low mass companion objects from our analysis. Treating binaries as single object also affects the relative strength of $H\alpha$ emission, which is discussed in § 5. LHS 1070 is a resolved triple system (M5.5, M8.5, and L0) where the primary is excluded by our spectral type criterion, but the M8.5 and L0 are part of the 2MUPM sample (Leinert et al. 2000).

Six objects are excluded from the 2MUPM sample because their optical magnitudes were too faint to obtain or measure a proper motion; one object was too close to another source to measure an accurate position. The proper motion measurements are discussed further in § 3.1. With the exclusion of 7 objects without proper motions and 11 low mass companion objects without resolved spectroscopy, the remaining 152 objects (81 M and 71 L) comprise the 2MUPM sample analyzed in this paper.

3. Measurements

3.1. Proper Motions and Tangential Velocities

When combined, 2MASS and DSS enable accurate, long baseline proper motion measurements for most 2MUPM systems—DSS images are from as early as 1950, while 2MASS coordinates and infrared images are from between 1997 and 2002. From the 159 2MASS selected M7–L8 dwarfs within 20 pc, we measured proper motions for 81 of 82 M dwarfs and 66 of 77 L dwarfs using DSS data as the first epoch and 2MASS coordinates as the second. The proper motion measurements adopted in this paper are a balance between the longest possible baseline and the best quality image. For 20% of the sample, POSS I data (baseline of 40–50 years) was used. Ten percent of the proper motions were measured using UK Schmidt data (16–24 years). The remaining proper motions were measured mainly from POSS II data with baselines of 2–16 years (20% with baselines <5 years).

While many of these objects were visible in multiple epochs of DSS data, eleven late-L dwarfs (2 L6, 5 L7, 4 L8) are not visible in any DSS band due to their faint optical magnitudes. One proper motion is available in existing literature; we use the measurement from Vrba et al. (2004) for 2MASS J01075242+0041563. Data

were obtained to measure proper motions of four of the remaining faint L dwarfs. The proper motions for 2MASS J1043075+222523 and 2MASS J2325453+425148 were measured with 2MASS data as the first epoch and deep, high resolution Gemini acquisition images from our 2004B program (Program ID: GN-2004B-Q-10) as the second epoch. For 2MASS J02572581–3105523 and 2MASS J0439010–235308, we used data from the CPAPIR camera on the CTIO 1.5m to provide second epoch astrometry. We exclude the remaining 6 L dwarfs (1 L6, 5 L7) from the 2MUPM sample. We also exclude one M8.5 dwarf because it is too close to a background star to measure an accurate position.

For each object, multiple band DSS images were obtained from the Canadian Astronomy Data Centre or, in four cases, another image was acquired of the target and surrounding field. Additionally, a list of 2MASS coordinates for nearby reference stars was obtained from the NASA/IPAC Infrared Science Archive using the GATOR interface. Proper motions were then measured using a custom IDL code. For each object, a transformation matrix between DSS image x,y coordinates and 2MASS frame RA,dec is calculated using the positions of reference stars surrounding the proper motion source. The position of the source in DSS image x,y coordinates is then translated into 2MASS frame RA,dec using the transformation matrix. The proper motion is solved for by comparing the translated first epoch coordinates with the 2MASS coordinates. Uncertainties in the proper motion measurements are calculated from the residuals between the transformed coordinates and the 2MASS coordinates for the reference stars; they are inversely dependent on the length of the baseline.

The tangential component of space velocity (V_{tan}) is the product of proper motion and distance. Our distances are calculated from the spectral type/ M_J relation found in Paper V. Proper motions, distances, and derived tangential velocities are given in Table 1. The V_{tan} distribution has a mean of $\langle V_{tan} \rangle = 31.3 \text{ km s}^{-1}$ and a dispersion of $\sigma_{tan} = 20.8 \text{ km s}^{-1}$. Kinematic results are discussed in more detail in § 4. Most objects in our sample have V_{tan} less than 100 km s^{-1} and the two kinematic outliers ($V_{tan} > 100 \text{ km s}^{-1}$) are discussed in § 4.2.

It was not possible to measure complete UVW kinematics for the 2MUPM sample. The spectra were not obtained with the goal of measuring radial velocities; they are from a variety of telescopes and conditions. Radial velocities require more consistent data. Additionally, the spectra for fainter dwarfs do not have sufficient signal-to-noise to measure radial velocities so the sample would be incomplete in later spectral types. While the lack of complete space motions does effect our analysis of individual objects, it should not drastically effect the kinematics of the population (Silvestri et al. 2002).

Proper motions were previously published for 95 of the 152 objects in the 2MUPM sample. We compared these measurements with ours to perform a check on our method of measuring proper motions. For 44 objects, measurements were made by either astrometric studies (Monet et al. 1992; Tinney, Reid, Gizis, & Mould 1995; Tinney 1996; Dahn et al. 2002; Vrba et al. 2004) or kinematic studies (Gizis et al. 2000; Deacon et al. 2005). Additionally, 80 of the 152 objects, proper motions were published in the USNO-B astrometric catalog (Monet et al. 2003). Our measurements are plotted against previous measurements in Figure 2.

The USNO-B measurements are not completely consistent with ours. Seventy of 80 objects agree within 0.1 '' yr^{-1} . Of the remaining 10, five agree within 0.2 '' yr^{-1} , and five did not agree (within $<0.2 \text{ '' yr}^{-1}$; these are not included in Figure 2). The automated methods used to measure proper motions for the USNO-B catalog are prone to mismatches; we prefer our proper motions as each measurement has been verified by eye.

Comparison with other works shows good agreement; our measurements are within 0.1 '' yr^{-1} of previous μ_{tot} and 10° of previously measured position angle. The one exception is SIPS 1936–5502, which we measure at $\mu_{tot} = 0.29 \pm 0.31 \text{ '' yr}^{-1}$, PA= 131° (with a three year baseline) and Deacon et al. (2005) measure at $\mu_{tot} = 0.84 \pm 0.05 \text{ '' yr}^{-1}$, PA= 134° . It is possible that our measurement is not entirely correct due to the short baseline, but we retain the object in our sample as it would be included in the absence of a comparison measurement. Generally, the proper motions found by parallax studies are more accurate, but we use our own measurements

for consistency.

Twenty-one of the 60 objects analyzed by Gizis et al. (2000) were re-observed as part of the 2MUPM sample. The proper motions show agreement within $0.06'' \text{ yr}^{-1}$ (within our uncertainties) but the V_{tan} comparison is less consistent. The distance estimates in Gizis et al. (2000) are based on $J - K_S$ color while our distances are derived from a spectral type/ M_J relation. The latter method yields improved distances (accurate to $\sim 10\%$) and thus more precise kinematics. For example, the maximum V_{tan} of 141 km s^{-1} in Gizis et al. (2000) was reduced to 97.9 km s^{-1} due to the revised distance estimate.

3.2. Spectral Features

An optical spectrum (6000–10000Å) for almost every object in the 2MUPM sample was obtained in order to assign spectral types (Papers V, IX, and X). Most (132) spectra examined for this analysis were obtained for the classification of the 2MASS selected samples, but some spectra from other sources were used. Spectral references are given in Table 2. Of the 152 2MUPM objects, there were 150 optical spectra available. Two dwarfs, 2MASS J01550354+0950003 and 2MASS J14283132+5923354 were confirmed and spectral typed using infrared spectra and we have not yet obtained optical spectra.

The *splot* routine in IRAF was used to visually inspect each spectrum and measure H α equivalent width (EW) and line flux. H α emission was detected in 63 of 81 M dwarfs and 15 of 69 L dwarfs, and upper limits were placed on H α non-detections by measuring the EW of a representative noise spike. Because emission strength for mid- to late-L dwarfs can be as small as $1\text{-}2\text{\AA}$, we consider objects with H α emission distinguishable from noise as active rather than establishing a cut-off between active and inactive.

We combined H α line flux with bolometric flux to obtain $\log(F_{H\alpha}/F_{bol})$. Bolometric fluxes were calculated for each object using 2MASS K_S magnitudes and the bolometric correction (BC_K) for K_S magnitudes found by Golimowski et al. (2004). BC_K is calculated from the polynomial fit to a spectral type/bolometric magnitude relation. For two objects, we were able to obtain H α EW but not line flux because the spectra were

not flux calibrated. H α measurements and upper limits are presented in Table 2, and the activity properties of the 2MUPM sample are discussed in detail in § 5.

For binary objects unresolved in 2MASS, the bolometric flux is calculated from the combined magnitude. This presents a problem when measuring H α emission from the combined spectra because we do not know what fraction of the total activity is emitted by which component. If one dwarf is active and the other inactive, the ratio of measured H α flux to the combined bolometric flux results in a smaller relative emission strength than would be calculated for the single active dwarf. Because we use the log of a ratio to indicate H α strength, the resulting uncertainty depends on the relative contributions of each component to the bolometric flux, which in turn depends on δK_S (the difference of the magnitudes).

If both components have equal emission strengths and K_S magnitudes, then the measured $\log(F_{H\alpha}/F_{bol})$ will be correct. For an equal mass binary with one active and one inactive component, $\log(F_{H\alpha}/F_{bol})$ is 0.30 dex lower than it would be for the single active object. The effect will be smaller for an unequal mass binary; for $\delta K_S = 2$ and activity only from the more luminous object, our calculated $\log(F_{H\alpha}/F_{bol})$ is 0.08 dex lower than it would be for the single active object. In Figures 6 and 7, binaries are plotted as shaded symbols with the maximum uncertainties resulting from the combined magnitudes (+0.30 dex). The LHS1070 system has resolved spectroscopy and there is no uncertainty as to which component is producing H α emission. We used relative photometry from Ratzka et al. (2007, in prep) to determine the bolometric flux of the B and C components, and measured H α from resolved spectroscopy (Leinert, priv. comm.).

The wavelength range of our optical spectra enabled examination of the 2MUPM sample for the Li I absorption line. According to the ‘‘lithium test,’’ the detection of the Li I absorption feature is a sufficient, but not necessary, indicator of substellar mass (Rebolo et al. 1992; Basri 1998). We have detected Li I in 3 of the 69 L dwarfs in the 2MUPM sample, which is a significantly smaller fraction than the one third found in the Kirkpatrick et al. (1999) sample of 25 L dwarfs. This disparity is likely due to the lower signal-to-

noise ratio of our spectra (obtained mostly with 4-m telescopes), compared to the Kirkpatrick et al. (1999) Keck 10-m spectra, so the small number of Li I detections is likely an observational effect rather than a physical property. Individual objects with Li I detections are discussed in papers V, IX, and X but there are not sufficient detections to use Li I as an age diagnostic in the 2MUPM sample.

For the objects that overlap with the Gizis et al. (2000) sample, comparison of our H α EW measurements yields some interesting differences. Of 21 objects, 15 had comparable (within 3 Å) H α EW measurements. Three of the six dwarfs with significantly different measurements have been observed in flare and are discussed in § 6.2. The other three objects have differences of 6–15 Å. It is likely that these differences are evidence of variability rather than the result of different signal-to-noise or measuring techniques. Measurements for these three objects which show smaller variations are listed with those of objects showing stronger variability in Table 3. For objects observed in both flare and quiescence, the quiescent measurement is used for sample statistics. We discuss activity properties of the 2MUPM sample in § 5 and variable activity in § 6.2.

4. Kinematics

4.1. Overall Properties

The photometric selection of the 2MUPM sample provides an opportunity to study kinematics without bias and derive age estimates from a well-defined sample. The 2MUPM sample is characterized by a mean tangential velocity of $\langle V_{tan} \rangle = 31.5 \text{ km s}^{-1}$ and a velocity dispersion of $\sigma_{tan} = 20.7 \text{ km s}^{-1}$. There are two outliers ($V_{tan} > 100 \text{ km s}^{-1}$) excluded from the kinematic analysis; these fast moving dwarfs are discussed in § 4.2. The mean velocity and velocity dispersion show good agreement with the kinematics of the Gizis et al. (2000) sample.

To obtain a kinematic age estimate for the 2MUPM sample, we use σ_{tan} to estimate the total velocity dispersion (σ_{tot}) with the equation $\sigma_{tot} = (3/2)^{1/2} \sigma_{tan}$. Velocity dispersion is converted to age using the relation found by Wielen (1977)

$$\sigma_{tot} = (10 \text{ km/s}) \times [1 + t/\tau]^{1/3}$$

where $\tau = 2 \times 10^8 \text{ yrs}$ and t is mean population age in years. With $\sigma_{tan} = 20.8 \text{ km s}^{-1}$ (which excludes the outliers discussed in § 4.2), this relation yields an age estimate of 3.1 Gyr for the 2MUPM sample. This kinematic age is sensitive to the spectrophotometric distances used to calculate V_{tan} . Allowing for the possibility of a systematic 10% over- or underestimation of the distances, we calculate that age estimates could vary from 2.2–4.2 Gyr. This is in excellent agreement with the kinematic age estimate of 2–4 Gyr found by Dahn et al. (2002).

We can use kinematics to further investigate the age distribution of M and L dwarfs. Monte Carlo simulations of the substellar mass function by Burgasser (2004) produce a modeled age distribution with respect to T_{eff} , shown in his Figure 8. Though there is a large spread of ages in each spectral type/temperature bin, the general trend shows an older mean age for late-M and early-L dwarfs and a younger mean age for late-L dwarfs. This is because the L spectral class encompasses a combination of stellar and substellar objects. Only younger, relatively warm brown dwarfs have T_{eff} that corresponds to L spectral types. Stars can have spectral types as late as \sim L4 and are likely to be older than brown dwarfs with the same T_{eff} (Burrows et al. 2001). One might expect that the combination of both younger brown dwarfs and older stars in late-M to early-L types would produce a wider velocity distribution while late-L types contain exclusively brown dwarfs and would have a narrower distribution.

To compare the expected ages with the kinematic distribution of the 2MUPM sample, we plot V_{tan} as a function of spectral type (Figure 3). We also plot the mean velocity and standard deviation for each spectral type bin to aid kinematic interpretation. Across M7 to L8 spectral types, the mean velocities per spectral type are largely constant. They are scattered within a range of $\langle V_{tan} \rangle = 15 \text{ km s}^{-1}$ to $\langle V_{tan} \rangle = 35 \text{ km s}^{-1}$, but there is no recognizable trend that hints at the expected age distribution.

Figure 4 shows velocity distribution histograms of the M7–L2 and L3–L8 populations. Both distributions peak at the bin centered on 25 km s^{-1} , and the velocity dispersions of the populations are nearly equal (M7–L2 with $\sigma_{tan} = 20.8 \text{ km s}^{-1}$ and L3–L8 with $\sigma_{tan} = 21.0 \text{ km s}^{-1}$), implying no age

difference. It is possible that the 2MUPM sample is too small for kinematics to distinguish between stars and brown dwarfs, but it is also likely that the age effect is not pronounced enough to be apparent in kinematics.

4.2. Kinematic Outliers

The three fastest objects in the 2MUPM sample warrant additional discussion. The fastest dwarf is 2MASS J1721039+334415 (hereafter 2M1721+33), an L3 with a velocity of $V_{tan} = 138.8 \pm 15.1 \text{ km s}^{-1}$; the next fastest is 2MASS J02511490-0352459 (hereafter 2M0251-03), an L3 with a velocity of $V_{tan} = 124.6 \pm 13.1 \text{ km s}^{-1}$; and third fastest is 2MASSW J1300425+191235 (hereafter 2M1300+19), an L1 dwarf with a velocity of $V_{tan} = 97.9 \pm 7.2 \text{ km s}^{-1}$. Both 2M0251-03 and 2M1721+33 are 4σ faster than the mean and are excluded from our kinematic analysis. While 2M1300+19 also has a high velocity, it is not as unusual as the two kinematic outliers and is included in our kinematic analysis.

In addition to their fast velocities, 2M1300+19 and 2M1721+33 are also unusually blue for their spectral types. Bluer colors suggest low metallicity and old dwarfs are likely to have high velocities. Gizis et al. (2000) discussed 2M1300+19 because the combination of its unusually blue color and high velocity indicate that it is likely to be old. Our calculated $V_{tan} = 97.9 \text{ km s}^{-1}$ is the third fastest velocity in the 2MUPM sample. Both 2M1200+19 and 2M1721+33 are discussed and spectra are presented in Papers V and IX because the combination of their slightly blue colors and faster kinematics suggest thick disk membership.

The remaining outlier, 2M0251-03, is also on the blue end of the color distribution but does not have unusual colors like 2M1300+19 and 2M1721+33. The spectrophotometric distance used to calculate its V_{tan} is $d_{phot} = 12.1 \pm 1.1 \text{ pc}$, which is consistent with a preliminary distance of $d = 12.7 \pm 1.2 \text{ pc}$ found by the CTIOPI parallax program (Bartlett 2006, priv. comm.). Our measured proper motion of $\mu = 2.17 \pm 0.11'' \text{ yr}^{-1}$ at $PA = 149 \pm 2^\circ$ is consistent with the proper motion of $\mu = 2.19 \pm 0.06'' \text{ yr}^{-1}$ at $PA = 149^\circ$ measured by Deacon et al. (2005). Tangential velocity is only two of the three components of the total velocity, and a slow radial velocity would place 2M0251-03 closer to the mean of the kinematic distribution.

While 2M0251-03 may be an unusual object, it is likely that its high velocity is simply the tail of the disk kinematic distribution.

5. Activity

5.1. Activity and Spectral Type

Previous work has shown that the presence and strength of $H\alpha$ emission in late-M and L dwarfs decreases with lower mass and later spectral type. Figure 5 plots the fraction of active objects per spectral type for the 2MUPM sample. M7 dwarfs have the largest activity fraction, with 21 of 22 objects (95%) showing $H\alpha$ emission. The activity fraction declines with later spectral type, but it does not go to zero. $H\alpha$ emission is present in 4 of 50 dwarfs between spectral types L2 and L8.

We find that the activity fraction of the 2MUPM sample drops rapidly through L dwarf sub-types. Half of L0 dwarfs are active, one-fifth to two-fifths of L1 dwarfs, and approximately one-tenth for spectral types L2 and later. While there is no doubt that the activity fraction drops, it is possible that the steepness of the drop is due to small numbers and observational effects rather than the activity properties of L dwarfs. For spectral types L3 and later, $H\alpha$ was only detected in spectra taken with 8-m or 10-m telescopes. The EW of those detections is smaller than the upper limit of most spectra taken with smaller telescopes. Gizis et al. (2000) suggest that a lowered continuum surrounding the $H\alpha$ emission feature should make up for the decreased sensitivity, but to fully investigate the activity properties of late-L dwarfs, higher signal-to-noise spectra are needed. While there are only a few $H\alpha$ detections for types L2 to L8, activity has been detected in at least three T dwarfs (Burgasser et al. 2003).

The peak activity fraction at M7 is consistent with previous results. Gizis et al. (2000) (Figure 6) found that all M7 and M8 dwarfs in their sample are active. Their activity fraction declines with later spectral type and no $H\alpha$ emission is found in types L5 and later. West et al. (2004) (Figure 1) found that 73% of M8 dwarfs in their sample show $H\alpha$ emission and the activity fraction similarly declines with later spectral type. They investigate the possibility that their maximum activity fraction is lower (73% rather than 100%) due to the Galactic distribution of their

sample. The West et al. (2004) sample, photometrically selected from SDSS with distances as large as 200 pc, includes a kinematically older portion of dwarfs due to its larger mean scale height above the Galactic disk. The distance limits of the 2MUPM sample and the Gizis et al. (2000) sample (20 pc and 25 pc) exclude dwarfs with large scale heights and thus include a younger population.

Though EW is a standard way to characterize emission and absorption features, it is not an accurate measure of activity strength across all ultracool spectral types. The continuum flux surrounding the $H\alpha$ feature decreases with later spectral type for M and L dwarfs, so the ratio of $H\alpha$ line flux to bolometric flux is used instead of EW to compare the strength of $H\alpha$ emission across a wide range of spectral types (Reid et al. 1995). Our method for computing $\log(F_{H\alpha}/F_{bol})$ is discussed in § 3.2.

Early-type M dwarfs, like solar-type stars, are generally believed to be powered by rotational dynamos, driven via the interface between the rotational core and the convective outer envelope (Parker 1955). M dwarfs become fully convective at spectral type $\sim M3$, and activity in later-type stars is attributed to a turbulent dynamo (Durney et al. 1993). However, the chromospheric activity distribution gives no indication of this transition: the average level of activity for M1 to M5 dwarfs with detected H-alpha remains constant at $\langle \log(F_{H\alpha}/F_{bol}) \rangle = -3.7$ (Hawley et al. 1996; West et al. 2004). At spectral types beyond M6, the activity level diminishes sharply (Martín et al. 1999; Gizis et al. 2000; Burgasser et al. 2002; Mohanty & Basri 2003; West et al. 2004).

Figure 6 shows activity strength plotted as a function of spectral type for the 2MUPM sample. Known multiple systems with unresolved spectroscopy are plotted at the spectral type of the primary with shaded symbols. As discussed in § 3.2, multiple systems (with the exception of LHS1070) are shown with an upper error bar that shows the maximum effect of using a combined magnitude to estimate bolometric flux. Taking this correction into account, the strength of emission from multiple systems appears to be the same as for single objects. The active B component of resolved binary LHS1070 is an M7.5 dwarf with a $\log(F_{H\alpha}/F_{bol}) = -4.67$, which does not fall above

the mean for its spectral type. The binary systems in the 2MUPM sample have estimated separations too large (1-10 AU) and estimated masses too small ($< 0.1M_{\odot}$) for any known binary interaction mechanism to enhance chromospheric activity (Cuntz et al. 2000; Burgasser et al. 2006). For the 2MUPM sample, binarity and activity are uncorrelated.

Activity strength shows a strong downward trend spanning spectral types M7–L5, which is consistent with previous results. This suggests a correlation between effective temperature and activity strength for this spectral type range. As discussed above, this downward trend begins at spectral type $\sim M6$, which is possibly correlated with a break down of the rotation/activity relation for earlier-type dwarfs (Basri 2001; Reid et al. 2002). Mohanty et al. (2002) find that the decrease is likely due to the high electrical resistivities in the cool, mostly neutral atmospheres of these ultracool objects, but the topic is still open to investigation.

5.2. Activity and Age

Solar-type main sequence stars exhibit a direct correlation between age and activity; this is generally attributed to rotational spin-down, and a consequent reduction in the energy output of the rotational dynamo. As noted in the previous section, mid- and late-type M dwarfs are fully convective, and are therefore not expected to show the same dependence between activity and rotation. Indeed, there is observational evidence that these late-type dwarfs exhibit different age-activity relationships (Gizas et al. 2000; Bochanski et al. 2005). For the 2MUPM sample, we find that there is a large scatter in the plot of $H\alpha$ emission strength ($\log(F_{H\alpha}/F_{bol})$) as a function of V_{tan} (Figure 7). Velocity is not a precise age indicator, but a loose correlation would be expected if ultracool dwarfs followed a solar-type activity-age relation.

Previous work has shown that active M dwarfs, as a population, have younger kinematics than inactive M dwarfs (Reid et al. 1995; Bochanski et al. 2005). To further investigate that activity/age relationship for late-M and L dwarfs, we plot velocity distributions of the 2MUPM sample with and without $H\alpha$ emission (Figure 8). The active dwarfs have a smaller velocity dispersion ($\sigma_{tan} =$

19.0 $km\ s^{-1}$) and a slightly slower peak ($\langle V_{tan} \rangle = 29.9\ km\ s^{-1}$) than the inactive dwarfs ($\sigma_{tan} = 22.8\ km\ s^{-1}$, $\langle V_{tan} \rangle = 33.3\ km\ s^{-1}$) which implies that the active dwarfs are younger than the inactive dwarfs. The velocity dispersions produce age estimates of ~ 2 Gyr and ~ 4 Gyr respectively. There is not a sufficient number of dwarfs, however, to conclude that the two populations have significantly different ages.

West et al. (2006) show that observations of SDSS M7 dwarfs are consistent with a constant level of activity followed by a rapid decrease in emission at an age of 6–7 Gyr. Further investigation indicates that this activity lifetime is longer with later spectral type (West et al., in prep). If this describes activity in the 2MUPM sample, then our population is too young (2–4 Gyr) to show the effect of age on activity.

To examine the kinematics in more detail, we plot the tangential velocity distributions of four different portions of the 2MUPM sample (Figure 9). These histograms divide spectral types M7-L2 (likely stellar) from L3-L8 (likely substellar) and H α emitters from non-emitters. The active M7-L2 population shows both a smaller σ_{tan} and a slower peak V_{tan} than both of the inactive distributions. However, a K-S test between the distributions indicates that there is no significant difference between the populations. Gizis et al. (2000) suggested, based on Li I detections, that active L dwarfs were drawn from an older, more massive population but the kinematics of the active L3–L8 dwarfs in our sample do not confirm this result. The active and inactive L dwarfs in the 2MUPM sample are kinematically indistinguishable, which is not surprising considering the small numbers of active L dwarfs. A larger sample would likely provide more insight into the age distribution of active L dwarfs.

6. Variable Activity

6.1. Variability in the 2MUPM Sample

Out of the 150 objects in the 2MUPM sample with optical spectra, there are 11 dwarfs that exhibit evidence of variability. Four of these have two observations with only 5–15 Å differences between the H α EW measurements. While their H α fluxes are not strong enough to classify them as flares, it is possible that this smaller scale vari-

ability is evidence that they are flaring objects not yet caught in peak flux. Both LHS 2065 and LP 412-31 have small scale variability as well as observed flare events. It is also possible that many more ultracool dwarfs have small scale variability but the effect has not yet been observed.

Seven dwarfs (5 M and 2 L) in the 2MUPM sample have been observed during flare events. Five (4 M and 1 L) were observed in flare as part of our observations of the 2MASS selected sample. If we assume that all objects in the 2MUPM sample are equally likely to flare, the number of objects observed in flare allows us to estimate that each dwarf spends 5/151 or $\sim 3\%$ of their time in flare. If we divide the sample by spectral type, the late-M dwarfs in our sample have a flare rate of 4/81 ($\sim 5\%$). Reid et al. (1999) found a flare rate of 7% through monitoring of BRI 0021, a M9.5 flare, and Gizis et al. (2000) similarly found a flare duty cycle of 7% for M7–M9.5 dwarfs.

Using the same logic for L dwarfs, we find a flare rate of 1/69 ($\sim 1\%$). This should be treated only as a lower limit due to the difficulty of observing weak H α in these faint objects. Many L dwarfs, especially spectral types L3 and later, only have one existing optical spectrum and not all those spectra have high enough signal-to-noise to observe H α at the expected strength for their spectral types (apprx. 1–2 Å). For L dwarfs with observed activity and one epoch of data, we have assumed emission is quiescent rather than the product of a flare event. There is also a possibility that early-L dwarfs are more likely to flare than late-L dwarfs, just as they are more likely to have quiescent emission. More observations, including higher signal-to-noise optical spectra and monitoring for variability, are needed to understand the activity properties of L dwarfs.

6.2. Variable Objects of Interest

2MASS J01443536–0716142 (hereafter 2M0144–07)

is an L5 that was observed during a flare event by Liebert et al. (2003) on 2001 Feb 20 with a maximum H α EW of 23 Å and on 2002 Jan 24 with no H α emission (upper limit 3 Å). Liebert et al. (2003) provide measurements of the H α as it declined from 24 Å to 6 Å over the course of 15 minutes. The spectrum of 2M0144–07 in flare shows no other emission lines, but if they are pro-

portionally weaker than the $H\alpha$ emission, they could be hidden under the noise.

LP 412–31 is a strongly flaring M8. We observed LP 412–31 on 2000 Oct 20 with an $H\alpha$ EW of 24 Å. On 2002 Jan 23 we observed it during a flare event with an $H\alpha$ EW of 330 Å and various other emission lines. These two spectra are plotted in Figure 10. Table 3 shows $H\alpha$ EW for a selection of other observations of LP 412–31, ranging from 18 Å to 83 Å (Reid et al. 2002; Basri 2001). The peak observed $H\alpha$ emission of 330 Å is more than a factor of 10 stronger than the weakest quiescent value. The recorded 83 Å emission could be part of a different flare event or it could be evidence of small-scale variability in addition to larger flare events. These variations have not been checked for periodicity.

LHS 2065 is an M9 that was observed in flare by Martín & Ardila (2001) (spectrum shown in their Figure 1) with a peak emission of 261 Å on 1998 Dec 12. LHS 2065 exhibits small scale variability (between 7 Å and 25 Å), both according to the other $H\alpha$ measurements presented in Martín & Ardila (2001) and our own measurements, listed in Table 3. This variability accompanied by a larger flare event is similar to the emission from the M8 dwarf LP 412–31, but the flare spectra for LHS 2065 is different because it shows $H\alpha$ with few other emission lines. Redward of $H\alpha$, the only additional emission is from the He I line, and it is only discernible in the epoch with the strongest $H\alpha$ emission.

LHS 2243 Gizis et al. (2000) observed this M8 dwarf in flare with an $H\alpha$ EW of 44 Å compared to a previous observation of 1.3 Å by Martín et al. (1994). We observed LHS 2243 on 11 June 2003 with an $H\alpha$ EW of 7 Å.

2MASSI J1108307+683017 (hereafter 2M1108+68) is an L0.5 dwarf that we observed on 2004 Mar 3 with no $H\alpha$ emission (upper limit 1 Å) but Gizis et al. (2000) observed it in 1999 Jun with an $H\alpha$ EW of 8 Å. Photometric variability studies in the I band have found

that 2M1108+68 is variable but not periodic (Gelino et al. 2002; Clarke et al. 2002). Gelino et al. (2002) suggest that the variability it is due to variations in the clouds at the surface of the dwarf and not activity. It is possible that the variable $H\alpha$ emission and the I band variations are both due to chromospheric activity, but more observations are needed to compare the photometric variations with the $H\alpha$ variability.

LHS 2397a is a spectroscopically unresolved binary system with an M8 dwarf primary and an L7.5 dwarf secondary (Freed et al. 2003). We observed LHS 2397 on 2002 Jan 23 with an $H\alpha$ EW of 78 Å, which is significantly stronger than the Martín et al. (1999) observation of 12 Å in 1998 Dec. Previously, Bessell (1991) observed strong variability in $H\alpha$ emission between two spectra taken 10 minutes apart in 1982.

2MASSW J1707183+643933 (hereafter 2M1707+64) is an M9 dwarf that we observed on 2003 Jul 7 with an $H\alpha$ EW of 28.7 Å. Gizis et al. (2000) also observed it in 1999 Jun with an EW of 9.8 Å. Rockenfeller et al. (2006a) examine the photometric variability of 2M1707+64 and find a period of ~ 3.6 hr, and Rockenfeller et al. (2006b) discuss photometric observations of this object during a particularly bright flare.

6.3. Strong $H\alpha$ Emission from the L1 dwarf 2MASS J10224821+5825453

We observed the L1 dwarf 2MASS J10224821+5825453 (hereafter 2M1022+58) on 2004 Feb 10 with an $H\alpha$ EW of 128 Å. The next two nights, 2004 Feb 11 and 12, the $H\alpha$ emission was at 24 and 26 Å, respectively. Figure 11 shows data from the three successive nights. The $H\alpha$ strength is enhanced by approximately an order of magnitude during the peak observed emission, but there are no other emission lines present. A lower signal-to-noise spectrum obtained on 2003 March 13 shows no $H\alpha$ emission with an upper limit of ~ 30 Å. Without more observations, it is difficult to classify 2M1022+58 as a flaring dwarf or as a consistently strong, variable emitter.

On the plot of spectral type vs. activity strength (Figure 6), 2M1022+58 is an outlier with remarkably strong quiescent emission of

$\log(F_{H\alpha}/F_{bol}) = -3.5$ (peak emission $\log(F_{H\alpha}/F_{bol}) = -2.7$). It is possible that the $\log(F_{H\alpha}/F_{bol}) = -3.5$ emission is not the quiescent level but is due to small-scale variability or another large variation. This relatively strong quiescent emission is evidence that 2M1022+58 is not a flaring dwarf but is in a permanent state of strong chromospheric activity.

There are three examples of consistently strong H α emission in the ultracool regime. The M9.5 star PC 0025+0447 (hereafter PC 0025) has been monitored for several years and shows continually strong activity at $\log(F_{H\alpha}/F_{bol}) \leq -3.4$ (Schneider et al. 1991; Martín et al. 1999). The limited observations of 2M1022+58 suggest similarities between the two objects, as H α emission in PC 0025 also varies by an order of magnitude. Hall (2002) suggest that the L3 dwarf 2MASS J1315309-264951 (hereafter 2M1315-26) shows similar strong, variable activity. It has been observed twice with an H α EW of ~ 120 Å ($\log(F_{H\alpha}/F_{bol}) = -4$), and two other epochs of spectroscopy show H α EWs of 97 Å and 25 Å. The third strong, variable dwarf is 2MASS J12373919+6526148 (hereafter 2M1237+65), a T6.5 dwarf monitored by Burgasser et al. (2002) which consistently shows unusually strong emission at $\log(F_{H\alpha}/F_{bol}) = -4.3$.

Aside from 2M1315-26 and 2M1022+58, there is only one other L dwarf that has been observed with variable activity. Liebert et al. (2003) observed the L5 dwarf 2MASS J01443536-0716142 (hereafter 2M0144-07) during a flare event with maximum H α emission at $\log(F_{H\alpha}/F_{bol}) = -4.6$. A later observation shows no H α emission. One unexpected similarity between these three variable L dwarfs is the absence of other emission lines that usually accompany variable H α emission. For 2M0144-07 and 2M1315-26, it is possible that other emission lines are present but simply below the noise. Emission lines in 2M1022+58, however, would be visible against the smooth continuum of the relatively high signal-to-noise spectra.

The H α emission in 2M1022+58 increases by a factor of 10 in our observations. When PC 0025 undergoes a similar increase, it is always accompanied by the appearance of some other emission lines, most notably He I. As an L1 with peak H α emission at least as strong as the emission of PC 0025, it is unknown why 2M1022+58 shows no

other emission lines.

The mechanism responsible for H α emission in 2M1022+58 warrants further investigation. Burgasser et al. (2002) and Martín et al. (1999) investigated the possibility of a tight, low mass companion object causing the variable, strong H α emission from 2M1237+65 and PC 0025 respectively. Neither investigation produced significant evidence of a companion object.

Liebert et al. (2003) hypothesized that H α emission from 2M0144-07 could be the result of an active dynamo in a relatively young, low mass object. Despite a fast tangential velocity of $V_{tan} = 81.9$ km s $^{-1}$, this L1 dwarf has optical spectral features that indicate youth (details are in Paper X). While the high V_{tan} suggests older age, it is based on only two of three velocity components. Kinematics are a good statistical age indicator but less accurate with single objects. For example, CM Draconis is a near-solar metallicity dwarf with a space velocity of 160 km s $^{-1}$ (Leggett et al. 1998; Viti et al. 2002). Further high signal-to-noise spectra should be obtained of this object, to characterize its variability, obtain a radial velocity, and determine whether significant lithium absorption is present.

6.4. An Amazing Flare Event on 2MASS J1028404-143843

During spectroscopic observations of the 2MASS selected sample, the M7 dwarf 2MASS J1028404-143843 (hereafter 2M1028-14) was observed during an amazing flare event; the flare spectrum and a comparison quiescent spectrum are plotted in Figure 12. On 2002 Jan 25 2M1028-14 was in flare with many emission lines, including H α with an EW of 97 Å, which is below 100 Å only because of the strongly enhanced flaring continuum. The EW and line fluxes for the flare observation are given in Table 4. Observations of 2M1028-14 in quiescence were taken on 2003 Mar 19 with an H α EW of 23 Å and on 2003 Mar 21 with an EW of 12 Å.

The 2M1028-14 flare event elevates the continuum well into the red optical spectra presented (6000 Å to ~ 10000 Å), to such an extent that the slope becomes blue. This effect is also found in the flare of 2MASS J0149089+295613 (hereafter 2M0149+29), an M9.5 star described in

Liebert et al. (1999). Observed over a similar wavelength region, the latter object also had an elevated continuum which extended from 6000 Å to ~ 7600 Å. Longward of 7600 Å, however, the photospheric molecular absorption of 2M0149+29 appeared relatively similar in strength to that in quiescence. The elevated continuum extends farther for 2M1028–14, where all but the strong 9400 Å H₂O band appear completely masked.

The emission spectra of both flaring objects contain lines varying in excitation from Ba II and He I to the neutral alkalis Na I and K I, which are typically in absorption but have been thrown into emission. Table 4 lists all the emission lines found in the flare spectrum. When scaled proportional to the H α feature, the emission spectrum of 2M1028–14 is weaker than that of 2M1049+29, except for the Ca II triplet.

It is difficult to compare the strength of the 2M1028–14 flare with the most active M dwarfs since the emphasis of previous studies has been on the ultraviolet and blue spectra plus H α . In these flare events, the erupting plasma reaches temperatures of order 10^4 K and forms a thermal bremsstrahlung continuum peaking in the far-ultraviolet (Giampapa 1983; Eason et al. 1992). Coordinated studies in the far-ultraviolet used the International Ultraviolet Explorer satellite with ground-based telescopes to measure this continuum component in the far-ultraviolet for flares in YZ CMi, Proxima Cen, and AD Leo (Foing et al. 1986). One of the most impressive of these coordinated studies was that of Hawley & Pettersen (1991) on “great flare of 1985 April 12 on AD Leonis.” These studies, however, provide no red optical spectra for direct comparison to 2M1028–14.

Liebert et al. (1999) argued that, if the ultraviolet flux scaled with H α in the same manner as it does in the M flare stars studied from space, 2M0149+29 emitted a flare luminosity that exceeded the normal bolometric photospheric luminosity at the flare’s peak. The same argument would apply to 2M1028–14, but the greater relative strength of the red continuum flux suggests that the flare’s peak luminosity could have exceeded that of the quiet photosphere even more than in the 2M0149+29 flare event.

We do not know whether the strongest M flare stars have red continua that turn blue like the 2M1028–14 event because we are not aware of an

observation where a flare continuum was studied at these wavelengths. More observations of these known flare stars in the optical would provide direct comparison, as would ultraviolet observations of 2M1028–14 in flare.

7. Summary

We have presented proper motions, tangential velocities, H α measurements, and flare observations for a nearly complete, volume limited sample of 152 late-M and L dwarfs. We summarize our results:

- The 2MUPM sample has a mean tangential velocity of $\langle V_{tan} \rangle = 31.5 \text{ km s}^{-1}$, and a tangential velocity dispersion of $\sigma_{tan} = 20.7 \text{ km s}^{-1}$. With the exception of two outliers, the distribution of tangential velocities is consistent with thin disk kinematics.
- Velocity distributions of the 2MUPM sample are not sufficiently sensitive to show the expected age distribution of stars and brown dwarfs. Examination of the Li I absorption feature is needed to further investigate the age distributions of stellar and sub-stellar populations.
- We find that there is no direct correlation between activity and age in the 2MUPM sample. Velocity distributions show that the active population is marginally older than the inactive population, but more data are needed to draw kinematic conclusions.
- In the 2MUPM sample, activity strength declines with later spectral type for types M7 and later; the correlation extends through L5 dwarfs.
- In agreement with previous results, we find the activity fraction to peak at spectral type M7 and decline through mid-L dwarfs for the 2MUPM sample. For spectral types L3 and later, the activity fraction is unclear due to the difficulty of obtaining high signal-to-noise spectra of these faint objects. More observations of L dwarfs are needed to understand the activity properties of these low mass objects.

- The late-M dwarfs in our sample have an estimated flare rate of $\sim 5\%$ which is consistent with previous results. We put a lower limit of $\sim 2\%$ on the flare rate of L dwarfs, but more data is needed to obtain a more accurate estimate and investigate the occurrence of flares across all L dwarf subtypes. It is possible, for example, that early-L dwarfs flare more often than late-L dwarfs.
- The L1 dwarf 2M1022+58 shows unexpectedly strong $H\alpha$ emission both in flare and quiescence. The absence of other emission lines in the flare spectrum remains unclear.
- The M7 dwarf 2M1028–14 shows an amazing flare spectrum with many emission lines.

We thank Adam Burgasser and Sebastian Levine for useful discussions. S. J. S. is partially supported by a grant from the New York NASA Space Grant Consortium, by NASA through an award issued by JPL/Caltech. This research was partially supported by a grant from the NASA/NSF NStars initiative, administered by JPL, Pasadena, CA. K. L. C. is supported by an NSF Astronomy and Astrophysics Postdoctoral Fellowship under award AST-0401418. Based on observations obtained at the Gemini Observatory, which is operated by the Association of Universities for Research in Astronomy, Inc., under a cooperative agreement with the NSF on behalf of the Gemini partnership: the National Science Foundation (United States), the Particle Physics and Astronomy Research Council (United Kingdom), the National Research Council (Canada), CONICYT (Chile), the Australian Research Council (Australia), CNPq (Brazil) and CONICET (Argentina). We gratefully acknowledge the team that built CPAPIR: Etienne Artigau, Rene Doyon and Daniel Nadeau. We also thank Etienne Artigau and Rene Doyon for continuing support of the instrument. CPAPIR was built through grants from the Canadian Foundation for Innovation and the Natural Science and Engineering Research Council of Canada. We thank the Research Consortium on Nearby Stars (RECONS) for a preliminary distance measured as part of the Cerro Tololo Inter-american Observatory Parallax Investigation (CTIOPI); CTIOPI was a National Optical Astronomy Observatory

(NOAO) Survey Program and continues as part of the Small and Moderate Aperture Telescope Research System (SMARTS) Consortium. This publication makes use of data products from the Two Micron All Sky Survey, which is a joint project of the University of Massachusetts and Infrared Processing and Analysis Center/California Institute of Technology, funded by the National Aeronautics and Space Administration and the National Science Foundation; the NASA/IPAC Infrared Science Archive, which is operated by the Jet Propulsion Laboratory/California Institute of Technology, under contract with the National Aeronautics and Space Administration. The Digitized Sky Survey was produced at the Space Telescope Science Institute under U.S. Government grant NAG W-2166. The images of these surveys are based on photographic data obtained using the Oschin Schmidt Telescope on Palomar Mountain and the UK Schmidt Telescope. The plates were processed into the present compressed digital form with the permission of these institutions. The National Geographic Society - Palomar Observatory Sky Atlas (POSS-I) was made by the California Institute of Technology with grants from the National Geographic Society. The Second Palomar Observatory Sky Survey (POSS-II) was made by the California Institute of Technology with funds from the National Science Foundation, the National Aeronautics and Space Administration, the National Geographic Society, the Sloan Foundation, the Samuel Oschin Foundation, and the Eastman Kodak Corporation. The Oschin Schmidt Telescope is operated by the California Institute of Technology and Palomar Observatory. The UK Schmidt Telescope was operated by the Royal Observatory Edinburgh, with funding from the UK Science and Engineering Research Council (later the UK Particle Physics and Astronomy Research Council), until 1988 June, and thereafter by the Anglo-Australian Observatory. The blue plates of the southern Sky Atlas and its Equatorial Extension (together known as the SERC-J), as well as the Equatorial Red (ER), and the Second Epoch [red] Survey (SES) were all taken with the UK Schmidt. Supplemental funding for sky-survey work at the ST ScI is provided by the European Southern Observatory. We accessed the Digital Sky as Guest User, Canadian Astronomy Data Centre, which is operated by the Herzberg Institute of Astro-

physics, National Research Council of Canada.

REFERENCES

- Basri, G. 1998, ASP Conf. Ser. 134: Brown Dwarfs and Extrasolar Planets, 134, 394
- Basri, G. 2001, ASP Conf. Ser. 223: 11th Cambridge Workshop on Cool Stars, Stellar Systems and the Sun, 223, 261
- Bessell, M. S. 1991, AJ, 101, 662
- Bochanski, J. J., Hawley, S. L., Reid, I. N., Covey, K. R., West, A. A., Tinney, C. G., & Gizis, J. E. 2005, AJ, 130, 1871
- Burgasser, A. J., Liebert, J., Kirkpatrick, J. D., & Gizis, J. E. 2002, AJ, 123, 2744
- Burgasser, A. J., Kirkpatrick, J. D., Liebert, J., & Burrows, A. 2003, ApJ, 594, 510
- Burgasser, A. J., Reid, I. N., Siegler, N., Close, L., Allen, P., Lowrance, P., & Gizis, J. 2006, ArXiv Astrophysics e-prints, arXiv:astro-ph/0602122
- Burgasser, A. J. 2004, ApJS, 155, 191
- Burrows, A., Hubbard, W. B., Lunine, J. I., & Liebert, J. 2001, Reviews of Modern Physics, 73, 719
- Costa, E., Méndez, R. A., Jao, W.-C., Henry, T. J., Subasavage, J. P., Brown, M. A., Ianna, P. A., & Bartlett, J. 2005, AJ, 130, 337
- Clarke, F. J., Oppenheimer, B. R., & Tinney, C. G. 2002, MNRAS, 335, 1158
- Cruz, K. L. & Reid, I. N. 2002, AJ, 123, 2828
- Cruz, K. L., Reid, I. N., Liebert, J., Kirkpatrick, J. D., & Lowrance, P. J. 2003, AJ, 126, 2421 (Paper V)
- Cruz et al. 2006, in press (Paper IX)
- Cuntz, M., Saar, S. H., & Musielak, Z. E. 2000, ApJ, 533, L151
- Dahn, C. C., et al. 2002, AJ, 124, 1170
- Deacon, N. R., & Hambly, N. C. 2001, A&A, 380, 148
- Deacon, N. R., Hambly, N. C., & Cooke, J. A. 2005, VizieR Online Data Catalog, 343, 50363
- Delfosse, X., et al. 1997, A&A, 327, L25
- Delfosse, X., et al. 2001, A&A, 366, L13
- Durney, B. R., De Young, D. S., & Roxburgh, I. W. 1993, Sol. Phys., 145, 207
- Eason, E. L. E., Giampapa, M. S., Radick, R. R., Worden, S. P., & Hege, E. K. 1992, AJ, 104, 1161
- Epchtein, N., et al. 1999, A&A, 349, 236
- ESA 1997, VizieR Online Data Catalog, 1239, 0
- Fan, X., et al. 2000, AJ, 119, 928
- Foing, B. H., et al. 1986, Revista Mexicana de Astronomia y Astrofisica, vol. 12, 12, 213
- Freed, M., Close, L. M., & Siegler, N. 2003, IAU Symposium, 211, 261
- Fuhrmeister, B., Schmitt, J. H. M. M., & Hauschildt, P. H. 2005, A&A, 436, 677
- Geballe, T. R., et al. 2002, ApJ, 564, 466
- Gelino, C. R., Marley, M. S., Holtzman, J. A., Ackerman, A. S., & Lodders, K. 2002, ApJ, 577, 433
- Giampapa, M.S. 1983, in "Activity in Red Dwarf Stars," eds. P.B. Byrne & M. Rodono (Dordrecht: Reidel), p 223
- Gizis, J. E., Monet, D. G., Reid, I. N., Kirkpatrick, J. D., Liebert, J., & Williams, R. J. 2000, AJ, 120, 1085
- Gizis, J. E. 2002, ApJ, 575, 484
- Gizis, J. E., & Reid, I. N. 1997, PASP, 109, 849
- Golimowski, D. A., et al. 2004, AJ, 127, 3516
- Hall, P. B. 2002, ApJ, 580, L77
- Hawley, S. L., Gizis, J. E., & Reid, I. N. 1996, AJ, 112, 2799
- Hawley, S. L., et al. 2002, AJ, 123, 3409
- Hawley, S. L., & Pettersen, B. R. 1991, ApJ, 378, 725

- Henry, T. J., Subasavage, J. P., Brown, M. A., Beaulieu, T. D., Jao, W.-C., & Hambly, N. C. 2004, *AJ*, 128, 2460
- Ianna, P. A., & Fredrick, L. W. 1995, *ApJ*, 441, L47
- Irwin, M., McMahon, R. G., & Reid, N. 1991, *MNRAS*, 252, 61P
- Jao, W.-C., Henry, T. J., Subasavage, J. P., Brown, M. A., Ianna, P. A., Bartlett, J. L., Costa, E., & Méndez, R. A. 2005, *AJ*, 129, 1954
- Kirkpatrick, J. D., Henry, T. J., & McCarthy, D. W., Jr. 1991, *ApJS*, 77, 417
- Kirkpatrick, J. D., Henry, T. J., & Simons, D. A. 1995, *AJ*, 109, 797
- Kirkpatrick, J. D., Henry, T. J., & Irwin, M. J. 1997, *AJ*, 113, 1421
- Kirkpatrick, J. D., et al. 1999, *ApJ*, 519, 802
- Kirkpatrick, J. D., et al. 2000, *AJ*, 120, 447
- Kirkpatrick, J. D., Liebert, J., Cruz, K. L., Gizis, J. E., & Reid, I. N. 2001, *PASP*, 113, 814
- Kirkpatrick et al. in prep
- Lasker, B. M., Doggett, J., McLean, B., Sturch, C., Djorgovski, S., de Carvalho, R. R., & Reid, I. N. 1996, *ASP Conf. Ser. 101: Astronomical Data Analysis Software and Systems V*, 101, 88
- Leggett, S. K., Allard, F., & Hauschildt, P. H. 1998, *ApJ*, 509, 836
- Leinert, C., Allard, F., Richichi, A., & Hauschildt, P. H. 2000, *A&A*, 353, 691
- Liebert, J., Kirkpatrick, J. D., Reid, I. N., & Fisher, M. D. 1999, *ApJ*, 519, 345
- Liebert, J., Kirkpatrick, J. D., Cruz, K. L., Reid, I. N., Burgasser, A., Tinney, C. G., & Gizis, J. E. 2003, *AJ*, 125, 343
- Martin, E. L., Rebolo, R., & Magazzu, A. 1994, *ApJ*, 436, 262
- Martín, E. L., Rebolo, R., & Zapatero-Osorio, M. R. 1996, *ApJ*, 469, 706
- Martín, E. L., Basri, G., & Zapatero Osorio, M. R. 1999, *AJ*, 118, 1005
- Martín, E. L., Delfosse, X., Basri, G., Goldman, B., Forveille, T., & Zapatero Osorio, M. R. 1999, *AJ*, 118, 2466
- Martín, E. L., & Ardila, D. R. 2001, *AJ*, 121, 2758
- Mohanty, S., Basri, G., Shu, F., Allard, F., & Chabrier, G. 2002, *ApJ*, 571, 469
- Mohanty, S., & Basri, G. 2003, *ApJ*, 583, 451
- Monet, D. G., Dahn, C. C., Vrba, F. J., Harris, H. C., Pier, J. R., Luginbuhl, C. B., & Ables, H. D. 1992, *AJ*, 103, 638
- Monet, D. G., et al. 2003, *AJ*, 125, 984
- Morgan, D. H. 1995, *ASP Conf. Ser. 84: IAU Colloq. 148: The Future Utilisation of Schmidt Telescopes*, 84, 137
- Parker, E. N. 1955, *ApJ*, 122, 293
- Phan-Bao, N., et al. 2001, *A&A*, 380, 590
- Phan-Bao, N., et al. 2003, *A&A*, 401, 959
- Ratzka, Leinert, & Allard 2007, in preparation
- Rebolo, R., Martin, E. L., & Magazzu, A. 1992, *ApJ*, 389, L83
- Reid, I. N., et al. 1991, *PASP*, 103, 661
- Reid, N., Hawley, S. L., & Mateo, M. 1995, *MNRAS*, 272, 828
- Reid, I. N., Kirkpatrick, J. D., Gizis, J. E., & Liebert, J. 1999, *ApJ*, 527, L105
- Reid, I. N., Kirkpatrick, J. D., Liebert, J., Gizis, J. E., Dahn, C. C., & Monet, D. G. 2002, *AJ*, 124, 519
- Reid, I. N., et al. 2003, *AJ*, 125, 354
- Reid, I. N., et al. 2007, in preparation (Paper X)
- Rockenfeller, B., Bailer-Jones, C. A. L., & Mundt, R. 2006, *A&A*, 448, 1111
- Rockenfeller, B., Bailer-Jones, C. A. L., Mundt, R., & Ibrahimov, M. A. 2006, *MNRAS*, 367, 407

Ruiz, M. T., Takamiya, M. Y., & Roth, M. 1991, ApJ, 367, L59

Ruiz, M. T., Leggett, S. K., & Allard, F. 1997, ApJ, 491, L107

Schneider, D. P., Greenstein, J. L., Schmidt, M., & Gunn, J. E. 1991, AJ, 102, 1180

Silvestri, N. M., Oswalt, T. D., & Hawley, S. L. 2002, AJ, 124, 1118

Silvestri, N. M., Hawley, S. L., & Oswalt, T. D. 2005, AJ, 129, 2428

Skrutskie, M. F., et al. 2006, AJ, 131, 1163

Skumanich, A. 1972, ApJ, 171, 565

Soderblom, D. R., Duncan, D. K., & Johnson, D. R. H. 1991, ApJ, 375, 722

Thorstensen, J. R., & Kirkpatrick, J. D. 2003, PASP, 115, 1207

Tinney, C. G., Reid, I. N., Gizis, J., & Mould, J. R. 1995, AJ, 110, 3014

Tinney, C. G. 1996, MNRAS, 281, 644

van Altena, W. F., Lee, J. T., & Hoffleit, E. D. 1995, The general catalogue of trigonometric [stellar] parallaxes (New Haven, CT: Yale University Observatory, c1995, 4th ed., completely revised and enlarged)

Viti, S., Jones, H. R. A., Maxted, P., & Tennyson, J. 2002, MNRAS, 329, 290

Vrba, F. J., et al. 2004, AJ, 127, 2948

West, A. A., et al. 2004, AJ, 128, 426

West, A. A., Bochanski, J. J., Hawley, S. L., Cruz, K. L., Covey, K. R., Silvestri, N. M., Reid, I. N., & Liebert, J. 2006, AJ, 132, 2507

Wielen, R. 1977, A&A, 60, 263

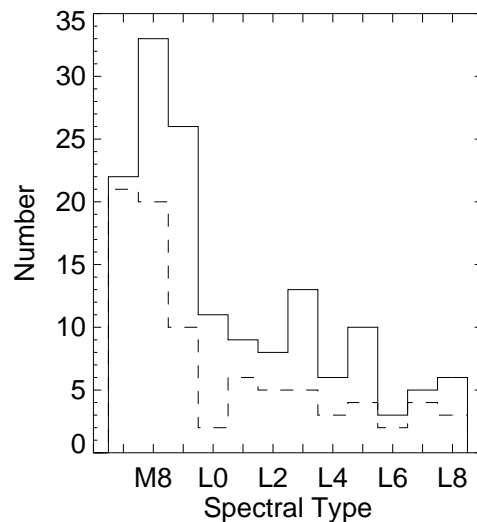


Fig. 1.— Spectral type distribution of the 2MUPM sample. The objects selected from the 2MASS second release (*dashed line*) and the objects selected from both the second and the all-sky release (*solid line*) are shown. A K-S test for types M8–L8 (see § 2) indicates no difference between the two spectral type distributions at the 90% significance level.

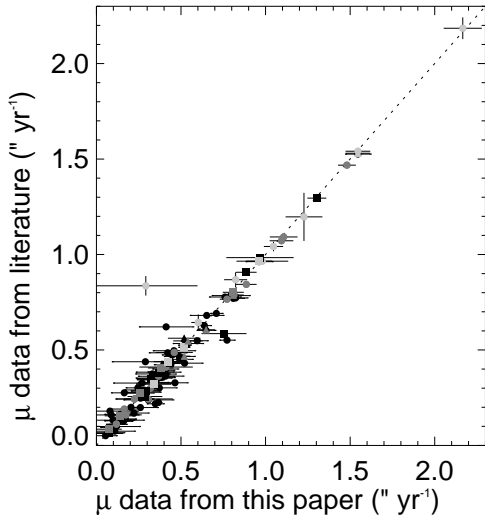


Fig. 2.— Proper motions from this paper vs. previously published measurements. The dotted line represents perfect agreement between the measurements. Data is plotted from the USNO-B catalog (*black circles*), Gizis et al. (2000, *dark grey circles*), Deacon et al. (2005, *light grey circles*), Dahn et al. (2002, *black squares*), Tinney, Reid, Gizis, & Mould (1995, *dark grey squares*), Tinney (1996, *light grey squares*), Thorstensen & Kirkpatrick (2003, *black triangles*), Monet et al. (1992, *dark grey triangles*), and Jao et al. (2005, *light grey triangles*).

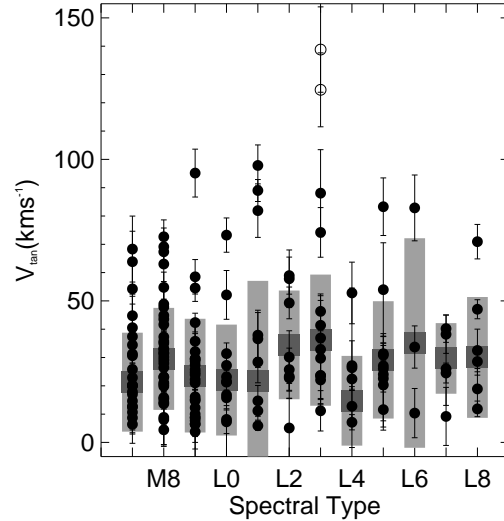


Fig. 3.— Spectral type vs. V_{tan} . Half-integer spectral types are rounded down. V_{tan} for the outliers (*open circles*) is distinguished from the data (*filled circles*) that is used to calculate the mean and dispersion. The mean V_{tan} (*squares*) and its associated one sigma deviation (*shaded bars*) are shown for each spectral type bin.

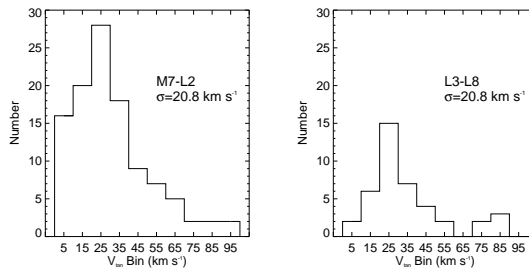


Fig. 4.— Distribution of V_{tan} for M7-L2 (*left*) and L3-L8 (*right*) dwarfs. The center of each 10 km s^{-1} wide bin is labeled. We find the dispersion (σ) to be 20.8 km s^{-1} for the M7-L2 portion of the sample, and 20.8 km s^{-1} for the L3-L8 portion. The histograms and the dispersions exclude the two outliers discussed in § 4.2 which are both L3 dwarfs with $V_{tan} > 100 \text{ km s}^{-1}$.

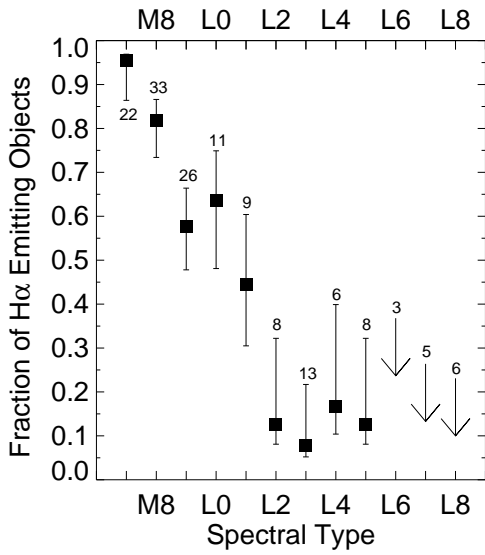


Fig. 5.— Fraction of objects with $H\alpha$ detection as a function of spectral type. The number above or below each data point is the total number of objects in each spectral type bin. The uncertainties are based on a binomial distribution. Upper limits are shown as down arrows for spectral type bins with no $H\alpha$ emitting objects.

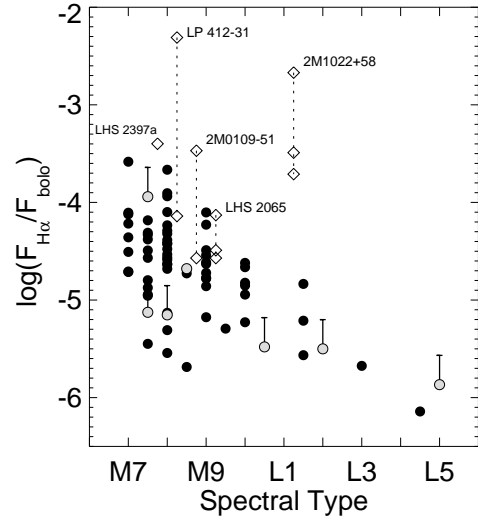


Fig. 6.— Log of the ratio of $H\alpha$ flux to bolometric flux as a function of spectral type for objects with $H\alpha$ detections. Multiple systems (*shaded circles*) are distinguished from single objects (*filled circles*). Multiple objects with unresolved spectroscopy are plotted with uncertainties that reflect the maximum uncertainty rising from the possibility that only one of the pair is active. Variable objects (*diamonds*) are labeled just above the strongest observed $H\alpha$ flux. They are plotted offset slightly from their spectral type with flare and quiescent emission connected by a dashed line. We include LHS 2065 though we did not observe it in peak flux. We only observed LHS 2397a during a flare event, so there is no quiescent data point.

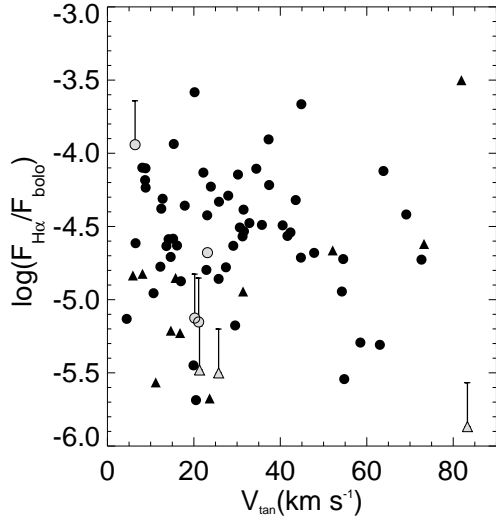


Fig. 7.— Relative H α flux vs. V_{tan} for active late-M dwarfs (*circles*) and L dwarfs (*triangles*) in the 2MUPM sample. Multiple systems (*shaded*) are distinguished from single objects (*black*). Multiple objects with unresolved spectroscopy are plotted with uncertainties that reflect the maximum uncertainty rising from the possibility that only one of the pair is active. Data for LHS 2397a is not plotted because our spectrum was taken while it was in flare.

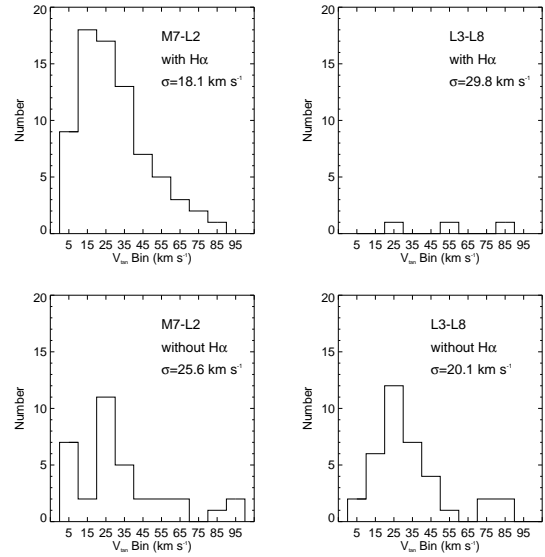


Fig. 9.— Distribution of V_{tan} for M7–L2 dwarfs with H α emission (*top left*), M7–L2 dwarfs without H α emission (*bottom left*), L3–L8 dwarfs with H α emission (*top right*) and L3–L8 dwarfs without H α emission (*bottom right*). The center of each 10 km s^{-1} wide bin is labeled and the σ of each distribution is given on each histogram. The histograms and the dispersions exclude the two outliers discussed in § 4.2 which are both inactive L3 dwarfs with $V_{tan} > 100 \text{ km s}^{-1}$.

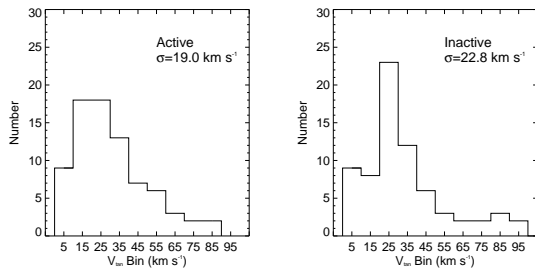


Fig. 8.— Distribution of V_{tan} for dwarfs with (*left*) and without (*right*) H α emission. We find a dispersion (σ) of 19.0 km s^{-1} for active dwarfs and 22.8 km s^{-1} for inactive dwarfs. A K-S test indicates no significant difference between the two populations. The histograms and the dispersions exclude the two outliers discussed in § 4.2 which are both inactive dwarfs with $V_{tan} > 100 \text{ km s}^{-1}$.

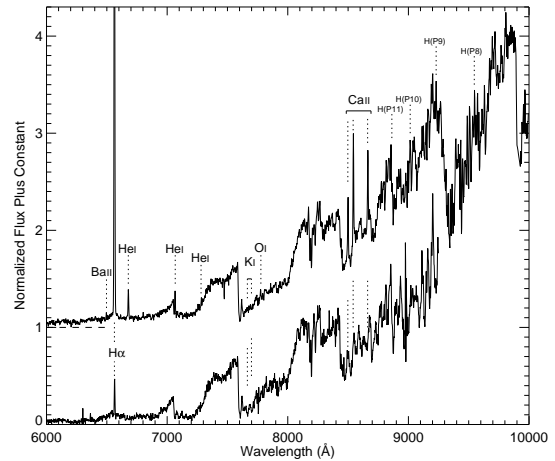


Fig. 10.— LP412–31, an M8 shown above in flare and below in quiescence. The dashed line marks the constant added to the flare spectrum. Various emission lines are labeled.

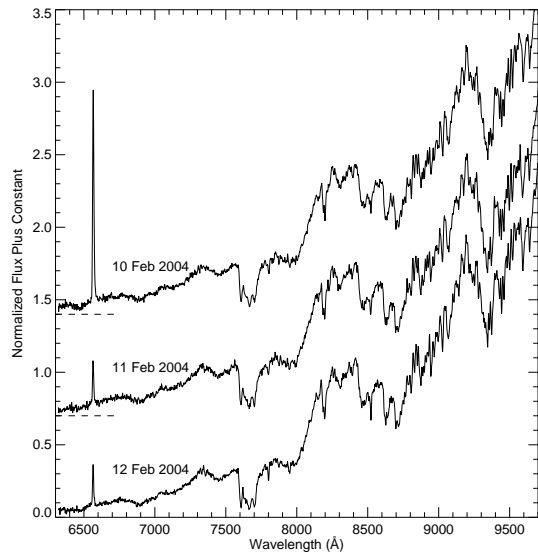


Fig. 11.— 2M1022+58, an L1 on three successive nights observed with large $H\alpha$ flare of EW 128 Å on 10 Feb 2004 and EW of 24 Å and 26 Å on the next two nights. The dashed lines mark the constants added to the offset spectra.

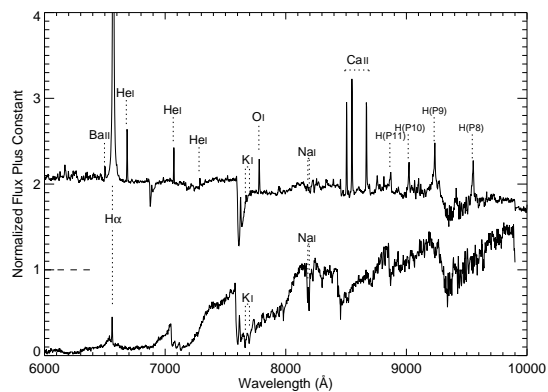


Fig. 12.— Spectacularly flaring 2M1028-14, an M7, shown above in flare and below in relative quiescence. The dashed line marks the constant added to the flare spectrum. Various emission lines are labeled.

TABLE 1
KINEMATICS OF THE 2MUPM SAMPLE

2MASS Designation	UCD #	Other Name	ST	d (pc)	μ_{tot} ($'' \text{ yr}^{-1}$)	PA ($^\circ$)	V_{tan} (km s $^{-1}$)	ST Ref.	π Ref.
00043484-4044058 ^a	20004	LHS 102B/GJ 1001B	L5	9.55± 1.04	1.83± 0.10	158± 3	83.3± 10.2	1	1
0019262+461407	10013	...	M8	19.50± 1.60	0.17± 0.06	124± 15	15.9± 5.7	2	
0019457+521317	10014	...	M9	18.70± 1.20	0.29± 0.20	111± 47	25.7± 17.5	2	
0024246-015819	10018	BRI 0021-0214	M9.5	11.55± 0.53	0.14± 0.09	338± 41	7.7± 5.1	3	2
0024442-270825	10019	LHS 1070b	M8.5	7.71± 0.14	0.63± 0.04	348± 5	23.1± 1.5	4	1,3
		LHS 1070c	L0						
0027559+221932 ^a	10022	LP 349- 25	M8:	10.30± 1.70	0.43± 0.05	113± 5	21.1± 4.1	5	
00315477+0649463	20024	LSPM J0031+06	M9	18.66± 1.22	0.28± 0.10	76± 11	24.7± 8.8	6	
00361617+1821104	20029	...	L3.5	8.76± 0.06	0.89± 0.06	83± 4	36.9± 2.6	1	
00413538-5621127	20035	DENIS-P J00041353-562112	M8	14.51± 1.19	0.12± 0.14	139± 56	8.1± 9.5	7	
00452143+1634446	20037	...	L0	18.44± 1.13	0.36± 0.04	102± 7	31.4± 3.8	6	
01025100-3737438	20049	LHS 132/LP 938- 71	M8	9.88± 0.81	1.47± 0.07	80± 4	69.1± 6.6	6	
01075242+0041563	20052	SDSS J010752.33+004156.1	L8	15.60± 1.10	0.63± 0.01 ^b	81.7± 0.3	47.1± 3.4	8	
01090150-5100494	20053	...	M9	14.21± 0.93	0.22± 0.11	65± 23	15.2± 7.5	6	
01092170+2949255	20055	...	M9.5	18.30± 1.13	1.09± 0.07	69± 3	95.2± 8.5	5	
01095111-034326	10068	LP 647- 13	M9	9.59± 0.21	0.35± 0.10	87± 6	16.1± 4.8	9	3
0123112-692138	13056	...	M8	17.20± 1.40	0.11± 0.12	107± 37	8.8± 9.6	10	
01282664-5545343	20068	...	L3	16.60± 1.50	0.30± 0.13	289± 20	23.6± 10.3	6	
0144353-071614	10088	...	L5	13.40± 1.50	0.49± 0.10	126± 11	31.3± 7.1	2	
0148386-302439	10091	...	M7.5	18.40± 1.80	0.15± 0.11	312± 33	12.8± 9.4	2	
01550354+0950003	20083	...	L5	17.95± 3.91	0.31± 0.07	95± 19	26.0± 8.2	6	
0205293-115930 ^a	10096	DENIS-P J0205.4-1159AB	L7:	19.76± 0.59	0.43± 0.05	83± 5	40.2± 4.8	11	4
0213288+444445	10102	...	L1.5	18.70± 1.40	0.17± 0.06	195± 21	14.7± 5.4	2	
02150802-3040011	20101	LHS 1367	M8	12.37± 1.02	0.81± 0.09	113± 6	47.8± 6.5	6	
02284243+1639329	20116	...	L0	19.37± 2.34	0.57± 0.06	141± 5	52.1± 8.6	6	
0248410-165121	10149	LP 771-21/BR 0246-1703	M8	16.23± 1.42	0.26± 0.09	190± 14	19.8± 7.0	12	5
0251148-035245	10151	...	L3	12.10± 1.10	2.17± 0.11	149± 2	124.6± 13.1	2	
0255035-470050	10158	DENIS-P J0255-4700	L8	4.90± 0.70	1.23± 0.11	120± 5	28.6± 4.8	13	
02572581-3105523	20139	...	L8	9.60± 0.60	0.71± 0.16	58± 13	32.5± 7.5	14	
03140344+1603056	20156	...	L0	14.43± 0.89	0.25± 0.07	254± 13	16.8± 4.9	6	
0320596+185423	10179	LP 412- 31	M8	14.54± 0.12	0.44± 0.05	125± 6	30.2± 3.7	15	3,4
03283463+1129515	20161	LSR J0328+1129	M8	18.26± 1.50	0.56± 0.05	64± 3	48.9± 6.0	6	
0331302-304238	10186	LP 888- 18	M7.5	12.10± 1.20	0.40± 0.06	182± 29	22.9± 3.9	2	
0339352-352544	10201	LP 944-20/BRI 0337-353	M9	4.97± 0.10	0.42± 0.08	49± 10	10.0± 2.0	12	5
0351000-005244	10213	LHS 1604	M7.5	14.68± 0.39	0.45± 0.06	177± 4	31.3± 4.2	2	1
03552337+1133437	20171	...	L6	10.13± 2.14	0.70± 0.05	159± 3	33.7± 7.5	6	
0417374-080000	10261	...	M7.5	17.40± 1.70	0.49± 0.09	96± 11	40.5± 8.4	2	
0423485-041403 ^a	10276	SDSS J042348.57-041403.5	L7:	15.17± 0.39	0.34± 0.05	283± 10	24.5± 3.5	10	7
0429184-312356 ^a	10287	...	M7.5:	11.40± 2.20	0.12± 0.06	46± 24	6.4± 3.4	2	
0435161-160657	10302	LP 775- 31	M7	8.60± 1.01	0.36± 0.03	25± 5	14.6± 2.1	2	
0439010-235308	10312	...	L6.5	10.80± 1.50	0.20± 0.17	220± 37	10.4± 8.7	2	
0440232-053008	10316	LP 655- 48	M7	9.80± 1.10	0.38± 0.08	66± 15	17.9± 4.1	2	
0443376+000205	10320	SDSS 0443+0002	M9:	16.20± 2.10	0.16± 0.08	146± 25	12.2± 6.2	16	
0445538-304820	10329	...	L2	16.60± 1.30	0.38± 0.11	161± 23	30.1± 9.3	2	
05002100+0330501	20197	...	L4	13.03± 1.35	0.36± 0.05	182± 9	22.4± 3.6	6	

TABLE 1—*Continued*

2MASS Designation	UCD #	Other Name	ST	d (pc)	μ_{tot} ($''$ yr $^{-1}$)	PA ($^{\circ}$)	V_{tan} (km s $^{-1}$)	ST Ref.	π Ref.
0517376–334902	10380	DENIS J051737.7–334903	M8	14.70± 1.20	0.60± 0.06	127± 5	41.6± 5.4	2	
0523382–140302	10390	...	L2.5	13.40± 1.10	0.08± 0.16	21± 105	5.1± 10.4	2	
0544115–243301	10444	...	M8	18.70± 1.60	0.71± 0.03	168± 2	63.0± 6.2	10	
06244595–4521548	20244	...	L5	15.31± 3.33	0.28± 0.19	19± 53	20.3± 14.9	6	
0652307+471034	10601	...	L4.5	11.10± 1.20	0.14± 0.05	336± 13	7.1± 2.7	2	
0700366+315726 ^a	10617	...	L3.5:	12.20± 0.30	0.52± 0.10	168± 13	29.7± 5.5	17	7
07075327–4900503	20258	ESO 207-61	M8	19.48± 0.85	0.38± 0.08	358± 10	35.0± 7.4	18	5,8
07140394+3702459	20263	...	M8	14.59± 1.20	0.20± 0.03	211± 7	14.2± 2.4	6	
0741068+173845	10666	LHS 1937	M7	17.90± 2.10	0.53± 0.05	200± 7	44.8± 6.9	19	
0746425+200032 ^a	10668	...	L0.5:	12.21± 0.04	0.37± 0.01	264± 4	21.3± 0.8	1	4
0752239+161215	10673	LP 423- 31	M7	10.50± 1.20	0.40± 0.05	153± 5	20.2± 3.5	2	
08040580+6153336	20290	...	M9	17.99± 1.17	0.64± 0.04	184± 2	54.5± 4.7	6	
08072607+3213101	20292	...	M8	15.94± 1.31	0.49± 0.08	233± 9	37.3± 6.5	6	
0818580+233352	10710	...	M7	19.10± 2.20	0.41± 0.16	229± 19	37.4± 15.0	5	
0825196+211552	10721	...	L7.5	10.66± 0.11	0.75± 0.13	251± 13	38.2± 6.8	1	4
08300825+4828482	20301	SDSS J083008.12+482847.4	L8	13.10± 0.61	1.14± 0.08	232± 3	70.9± 6.1	14	
08303256+0947153	20302	LHS 2021	M8	14.03± 1.15	0.67± 0.07	226± 5	44.9± 5.8	20	
0835425–081923	10742	...	L5	8.30± 0.90	0.61± 0.03	299± 3	24.0± 2.9	2	
0847287–153237	10764	...	L2	17.50± 1.40	0.27± 0.05	146± 10	22.8± 4.4	2	
0853362–032932	10776	LHS 2065	M9	8.63± 0.09	0.54± 0.09	248± 9	22.2± 3.6	21	3,9
0908380+503208	10802	...	L7	10.50± 1.50	0.52± 0.25	202± 21	26.0± 12.9	2	
09111297+7401081	20333	...	L0	17.30± 1.07	0.26± 0.04	230± 8	21.5± 3.9	6	
09153413+0422045 ^a	20335	...	L7	14.20± 2.50	0.14± 0.15	284± 84	9.2± 10.3	6	
09211410–2104446	20336	SIPS 0921–2104	L2	12.40± 1.01	0.98± 0.15	163± 10	57.8± 10.2	6	
09492223+0806450	20352	LHS 2195	M8.5	15.74± 1.13	0.90± 0.02	176± 2	67.3± 5.1	19	
1006319–165326	10877	LP 789–23	M7.5	16.40± 1.60	0.33± 0.10	304± 12	25.8± 8.1	2	
1016347+275149	10892	LHS 2243	M8	14.40± 1.20	0.46± 0.11	200± 10	31.5± 8.0	15	
10224821+5825453	20373	...	L1	19.94± 1.34	0.86± 0.08	205± 7	81.9± 9.4	6	
1024099+181553	10906	...	M8	16.50± 1.40	0.17± 0.09	241± 31	13.6± 7.5	5	
1043075+222523	10926	...	L8:	17.20± 4.01	0.14± 0.00	262± 0	11.8± 2.8	10	
1045240–014957	10929	SDSS J104524.00–014957.6	L1	16.80± 1.10	0.46± 0.12	266± 8	36.6± 10.1	16	
10481463–3956062	20385	DENIS-P J104814.7–395606	M9	4.02± 0.02	1.55± 0.07	228± 2	29.5± 1.4	22	3,10,
10484281+0111580	20387	SDSS J104842.81+011158.2	L1	15.30± 1.02	0.52± 0.10	241± 9	37.9± 8.0	16	
10511900+5613086	20388	...	L2	15.38± 2.38	0.32± 0.09	197± 23	23.3± 7.7	6	
10554733+0808427	20391	...	M8	19.01± 1.57	0.37± 0.01	255± 5	33.2± 3.0	6	
1058478–154817	10949	DENIS-P J1058.7–1548	L3	17.33± 0.30	0.29± 0.10	288± 15	23.6± 8.5	11	4
1104012+195921	10954	...	L4	18.80± 2.01	0.14± 0.08	24± 31	12.8± 6.9	2	
1108307+683017	10960	...	L0.5	18.01± 1.10	0.32± 0.04	230± 6	27.2± 4.0	5	
1121492–131308 ^a	10980	LHS 2397a	M8:	14.45± 0.29	0.52± 0.04	267± 11	35.7± 2.5	21	1,5,9
11395113–3159214	20419	...	M9	17.54± 1.15	0.08± 0.05	270± 51	6.5± 4.4	23	
11553952–3727350	20431	...	L2	12.60± 0.99	0.82± 0.07	176± 3	49.3± 5.6	23	
12035812+0015500	20433	SDSS J120358.19+001550.3	L3	18.47± 1.69	1.00± 0.15	257± 6	88.1± 15.4	24	
1213033–043243	11044	...	L5	16.70± 1.80	0.15± 0.09	260± 38	11.6± 7.3	2	
12212770+0257198	20444	...	L0	19.40± 1.19	0.09± 0.16	258± 76	8.1± 14.7	6	
1224522–123835	11068	BR 1222–1221	M9	17.06± 1.11	0.34± 0.10	245± 22	27.4± 8.6	15	5

TABLE 1—*Continued*

2MASS Designation	UCD #	Other Name	ST	d (pc)	μ_{tot} (″ yr ⁻¹)	PA (°)	V_{tan} (km s ⁻¹)	ST Ref.	π Ref.
1246517+314811	11095	LHS 2632	M7.5	18.10± 1.80	0.79± 0.11	273± 8	68.3± 11.7	15	
1253124+403403	11109	LHS 2645	M7.5	17.50± 1.70	0.65± 0.10	158± 7	54.2± 9.6	21	
1300425+191235	11115	...	L1	13.90± 0.90	1.48± 0.05	212± 2	97.9± 7.2	5	
1305401−254106 ^a	11122	Kelu-1	L2:	18.66± 0.70	0.29± 0.09	270± 22	25.7± 7.6	25	4
1309218−233035	11127	CE 303	M8	13.30± 1.10	0.37± 0.13	182± 24	23.1± 8.4	2	
1332244−044112	11153	...	M7.5	18.90± 1.80	0.10± 0.10	60± 41	8.7± 9.0	2	
1356414+434258	11177	LP 220- 13	M7	15.60± 1.80	0.46± 0.07	279± 8	34.4± 6.7	2	
1403223+300754	11188	...	M8.5	18.80± 1.40	0.81± 0.03	270± 5	72.7± 6.0	5	
1411213−211950	11194	...	M9	15.70± 1.01	0.12± 0.05	213± 16	8.8± 3.6	2	
14213145+1827407	20562	...	L0	19.96± 1.22	0.77± 0.04	257± 2	73.2± 6.1	5	
14252798−3650229	20568	DENIS-P J142527.97−36502	L3	16.39± 2.98	0.53± 0.10	204± 7	41.4± 11.1	6	
14283132+5923354	20570	...	L5	17.60± 3.80	0.27± 0.17	250± 32	22.6± 15.0	6	
14284323+3310391	20571	LHS 2924/ LP 271−25/ GJ	M9	11.01± 0.16	0.81± 0.06	201± 6	42.3± 3.3	21	
1438082+640836	11224	...	M9.5	18.40± 1.10	0.67± 0.06	107± 3	58.5± 6.1	2	
14392836+1929149	20581	...	L1	14.37± 0.10	1.30± 0.06	288± 1	89.0± 3.9	26	
1440229+133923	11230	LSPM J1440+1339	M8	17.60± 1.50	0.35± 0.05	202± 4	29.1± 4.7	10	
14482563+1031590	20587	...	L5	15.90± 3.50	0.71± 0.15	98± 13	54.0± 16.6	6	
1456383−280947	11264	LHS 3003	M7	6.70± 0.12	0.96± 0.08	212± 4	30.6± 2.5	15	3,5
15010818+2250020	20596	TVLM 513-46546	M9	10.59± 0.07	0.08± 0.08	223± 48	3.8± 3.8	15	
1506544+132106	11291	...	L3	14.10± 1.30	1.11± 0.08	274± 3	74.2± 8.8	5	
1507277−200043	11294	...	M7.5	14.20± 1.40	0.16± 0.05	98± 10	10.7± 3.7	2	
1507476−162738	11296	...	L5	7.33± 0.03	0.88± 0.06	186± 7	30.8± 2.0	1	4
15101685−0241078	20602	TVLM 868-110639	M9	16.34± 1.25	0.38± 0.08	271± 9	29.5± 6.3	15	
15104786−2818174	20604	...	M9	18.82± 1.24	0.10± 0.18	272± 174	8.8± 16.1	23	
1515009+484739	11314	...	L6	10.20± 1.40	1.71± 0.05	327± 1	82.9± 11.6	2	
1521010+505323	11323	...	M7.5	16.10± 1.60	0.22± 0.08	161± 16	17.0± 6.6	2	
1534570−141848	11346	...	M7	13.50± 1.60	1.00± 0.12	251± 5	63.9± 10.8	10	
15394189−0520428	20625	DENIS-P J153941.96−05204	L3.5	16.18± 1.59	0.60± 0.04	85± 7	46.3± 5.5	6	
15394442+7437273	20626	...	M9	19.64± 1.28	0.07± 0.09	326± 56	6.4± 8.7	6	
1546054+374946	11439	...	M7.5	19.70± 1.90	0.13± 0.09	174± 70	12.5± 8.1	5	
16073123−0442091	20660	...	M8	14.06± 1.15	0.42± 0.08	177± 14	27.9± 5.6	23	
16154245+0546400	20662	...	M9	19.18± 1.25	0.16± 0.07	139± 22	14.8± 6.3	6	
1658037+702701	11668	...	L1	18.55± 0.24	0.32± 0.08	207± 7	28.4± 7.3	5	4
17071830+6439331	20700	...	M9	16.40± 1.07	0.31± 0.14	121± 21	23.9± 11.4	5	
17072343−0558249 ^a	20701	...	L0:	13.80± 1.70	0.11± 0.06	66± 40	7.3± 4.2	23	
1721039+334415	11694	...	L3	15.20± 1.40	1.92± 0.11	287± 3	138.8± 15.1	2	
17312974+2721233	20744	...	L0	11.80± 0.70	0.28± 0.05	200± 5	15.8± 2.7	6	
17351296+2634475 ^a	20746	LSPM J1735+2634	M7.5:	11.42± 1.11	0.37± 0.10	150± 11	20.2± 5.8	6	
17534518−6559559	20760	...	L4	15.86± 3.26	0.36± 0.09	178± 24	27.1± 8.8	6	
1757154+704201	11735	LP 44-162	M7.5	12.50± 1.20	0.34± 0.09	2± 7	19.9± 5.6	5	
1807159+501531	11756	...	L1.5	14.60± 1.10	0.16± 0.05	167± 15	11.2± 3.3	2	
1835379+325954	11792	LSR J1835+3259	M8.5	5.67± 0.02	0.76± 0.09	183± 4	20.5± 2.5	27	12
1843221+404021	11800	LHS 3406	M8	14.14± 0.16	0.65± 0.05	352± 3	43.6± 3.6	2	9
18451889+3853248	20793	LSPM J1845+3853	M8	16.28± 1.34	0.41± 0.10	32± 11	31.6± 8.5	6	
19360187−5502322	20823	SIPS 1936−5502	L4:	19.00± 3.90	0.29± 0.31	131± 51	26.4± 28.2	6	

TABLE 1—*Continued*

2MASS Designation	UCD #	Other Name	ST	d (pc)	μ_{tot} ($''$ yr $^{-1}$)	PA ($^{\circ}$)	V_{tan} (km s $^{-1}$)	ST Ref.	π Ref.
20004841–7523070	20845	...	M9	17.90± 1.20	0.34± 0.07	220± 9	28.7± 6.1	6	
20282035+0052265	20866	SDSS J202820.32+005226.5	L3	17.40± 1.80	0.14± 0.09	105± 28	11.2± 7.1	16	
20360316+1051295	20870	...	L3	18.00± 1.65	0.26± 0.09	216± 21	22.1± 8.4	6	
2037071–113756	12027	...	M8	16.80± 1.40	0.41± 0.06	182± 15	32.8± 5.3	2	
20450238–6332066	20875	...	M9	17.01± 1.11	0.26± 0.10	159± 15	21.0± 8.3	6	
2057540–025230	12054	...	L1.5	15.70± 1.10	0.08± 0.02	171± 17	5.9± 1.6	2	
2104149–103736	12059	...	L2.5	18.70± 1.60	0.66± 0.05	115± 3	58.9± 6.5	14	
2224438–015852	12128	...	L4.5	11.49± 0.12	0.97± 0.20	150± 7	52.8± 10.9	1	4,6
22264440–7503425	20946	DENIS-P J222644.3–750342	M8	17.36± 2.83	0.05± 0.06	24± 60	4.5± 5.3	28	
2237325+392239	12145	G 216-7B	M9.5	18.89± 0.69	0.36± 0.07	181± 8	32.1± 6.4	29	13
22521073–1730134 ^c	20976	DENIS-P J225210.73–17301	L5.5	12.70± 1.70	0.45± 0.12	71± 10	27.0± 8.0	6	
22551861–5713056	20979	...	L3	19.14± 6.95	0.36± 0.14	207± 16	32.8± 17.3	6	
2306292–050227	12171	...	M8	11.01± 0.90	1.05± 0.06	117± 4	54.8± 5.4	5	
2325453+425148	13227	...	L8	14.10± 2.01	0.28± 0.10	180± 45	18.9± 7.2	10	
23464599+1129094	21011	LSPM J2346+1129	M9	18.47± 1.20	0.41± 0.07	261± 8	35.7± 6.9	6	
2349489+122438	12217	LP 523–55	M8	19.60± 1.60	0.16± 0.08	174± 37	15.3± 7.2	5	
2351504–253736	12220	...	M8	13.20± 0.80	0.42± 0.11	62± 15	26.4± 7.0	10	

NOTE.—Reference for π is only listed if the distance given is a parallax measurement.

^aBinary considered as a single object due to the lack of resolved spectroscopy.

^bProper motion from Vrba et al. (2004)

^cWide binary

References. — Spectral Type References: (1) Kirkpatrick et al. 2000 (2) Paper 5 (3) Irwin et al. 1991 (4) Leinert et al. 2000 (5) Gizis et al. 2000 (6) Paper 10 (7) Phan-Bao et al. 2001 (8) Geballe et al. 2002 (9) Cruz & Reid 2002 (10) Paper 9 (11) Delfosse et al. 1997 (12) Kirkpatrick et al. 1997 (13) Martín et al. 1999b (14) Kirkpatrick et al. in prep (15) Kirkpatrick et al. 1995 (16) Hawley et al. 2002 (17) Thorstensen & Kirkpatrick 2003 (18) Ruiz et al. 1991 (19) Gizis & Reid 1997 (20) Henry et al. 2004 (21) Kirkpatrick et al. 1991 (22) Delfosse et al. 2001 (23) Gizis 2002 (24) Fan et al. 2000 (25) Ruiz et al. 1997 (26) Kirkpatrick et al. 1999 (27) Reid et al. 2003 (28) Phan-Bao et al. 2003 (29) Kirkpatrick et al. 2001

References. — π References: (1) van Altena et al. 1995 (2) Tinney, Reid, Gizis, & Mould 1995 (3) Costa et al. 2005 (4) Dahn et al. 2002 (5) Tinney 1996 (6) Vrba et al. 2004 (7) Thorstensen & Kirkpatrick 2003 (8) Ianna & Fredrick 1995 (9) Monet et al. 1992 (10) Deacon & Hambly 2001 (11) Jao et al. 2005 (12) Reid et al. 2003 (13) ESA 1997

TABLE 2—*Continued*

2MASS Designation	UCD #	Other Name	ST	K	M_{bol}	F_{bol}	H α EW (Å)	H α Flux	$\log(F_{H\alpha}/F_{bol})$	UT date	Spectra Ref
0517376–334902	10380	DENIS J051737.7–334903	M8	10.82	13.92	7.65E-11	-5.13	2.08E-15	-4.56	2002 Jan 25	
0523382–140302	10390	...	L2.5	11.63	14.95	2.95E-11	> -0.78	2002 Jan 24	
0544115–243301	10444	...	M8	11.44	14.54	4.32E-11	-1.58	2.12E-16	-5.31	2002 Sep 25	
06244595–4521548	20244	...	L5	12.6	15.94	1.19E-11	> -9.92	2003 Apr 21	
0652307+471034	10601	...	L4.5	11.69	15.04	2.72E-11	> -2.90	2004 Feb 12	
0700366+315726 ^a	10617	...	L3.5:	11.31	14.65	3.88E-11	> -1.16	2004 Feb 10	3
07075327–4900503	20258	ESO 207-61	M8	12.11	15.20	2.34E-11	> -6.27	
07140394+3702459	20263	...	M8	10.84	13.93	7.51E-11	-7.33	1.95E-15	-4.59	2003 Mar 13	
0741068+173845	10666	LHS 1937	M7	10.97	14.02	6.92E-11	-3.94	1.34E-15	-4.71	2003 Mar 13	
0746425+200032 ^a	10668	...	L0.5:	10.49	13.72	9.16E-11	-1.80	3.03E-16	-5.48	...	
0752239+161215	10673	LP 423- 31	M7	9.82	12.87	2.00E-10	-36.22	5.21E-14	-3.58	2002 Jan 25	
08040580+6153336	20290	...	M9	11.45	14.60	4.06E-11	-9.53	7.69E-16	-4.72	2003 Mar 15	
08072607+3213101	20292	...	M8	11.05	14.15	6.18E-11	-20.93	7.68E-15	-3.91	2003 Mar 14	
0818580+233352	10710	...	M7	11.13	14.19	5.96E-11	-10.11	3.62E-15	-4.22	2003 Mar 13	
0825196+211552	10721	...	L7.5	13.05	16.28	8.65E-12	> -4.32	1998 Dec 14	6
08300825+4828482	20301	SDSS J083008.12+482847.4	L8	13.68	16.88	5.01E-12	> -1.60	
08303256+0947153	20302	LHS 2021	M8	10.76	13.85	8.10E-11	-28.23	1.75E-14	-3.66	2004 Feb 10	
0835425–081923	10742	...	L5	11.16	14.50	4.46E-11	> -3.54	2004 Feb 12	
0847287–153237	10764	...	L2	12.05	15.36	2.03E-11	> -1.11	2004 Feb 12	
0853362–032932	10776	LHS 2065	M9	9.97	13.12	1.59E-10	-8.13	1.17E-14	-4.13	2002 Jan 23	2
0908380+503208	10802	...	L7	12.92	16.19	9.44E-12	> -5.60	2002 Jan 22	
09111297+7401081	20333	...	L0	11.75	14.95	2.94E-11	> -3.31	2004 Feb 10	
09153413+0422045 ^a	20335	...	L7	13.01	16.28	8.66E-12	> 5.29	2004 Feb 11	
09211410–2104446	20336	SIPS 0921–2104	L2	11.69	14.99	2.83E-11	> -2.99	2003 Mar 13	
09492223+0806450	20352	LHS 2195	M8.5	11.21	14.33	5.23E-11	> -1.97	2003 Apr 22	
1006319–165326	10877	LP 789–23	M7.5	11	14.07	6.61E-11	-5.88	3.08E-15	-4.33	2002 Jan 26	
1016347+275149	10892	LHS 2243	M8	10.95	14.04	6.80E-11	-6.92	2.80E-15	-4.39	2003 May 15	
10224821+5825453	20373	...	L1	12.16	15.42	1.92E-11	-24	6.05E-15	-3.50	2004 Feb 10	
1024099+181553	10906	...	M8	11.21	14.30	5.36E-11	-7.72	1.25E-15	-4.63	2003 May 15	
1043075+222523	10926	...	L8:	13.99	17.19	3.75E-12	> -4.6	2004 Nov 7	
1045240–014957	10929	SDSS J104524.00–014957.6	L1	11.81	15.07	2.64E-11	> -17.68	2002 Jan 31	
10481463–3956062	20385	DENIS-P J104814.7–395606	M9	8.45	11.60	6.48E-10	-4.77	4.31E-15	-5.18	2003 May 14	
10484281+0111580	20387	SDSS J104842.81+011158.2	L1	11.62	14.88	3.14E-11	> -1.11	2003 Apr 21	
10511900+5613086	20388	...	L2	11.91	15.21	2.33E-11	> -2.31	2004 Feb 10	
10554733+0808427	20391	...	M8	11.37	14.46	4.61E-11	> -6.49	2003 Mar 15	
1058478–154817	10949	DENIS-P J1058.7–1548	L3	12.51	15.85	1.29E-11	-1.61	2.74E-17	-5.67	...	4
1104012+195921	10954	...	L4	12.98	16.32	8.31E-12	> -1.62	2002 Jan 22	
1108307+683017	10960	...	L0.5	11.6	14.83	3.29E-11	> -0.86	2004 Feb 12	
1121492–131308 ^a	10980	LHS 2397a	M8:	10.72	13.82	8.35E-11	-77.69	3.34E-14	-3.40	...	
11395113–3159214	20419	...	M9	11.5	14.65	3.88E-11	-11.84	9.43E-16	-4.61	2003 Apr 23	
11553952–3727350	20431	...	L2	11.46	14.76	3.50E-11	> -2.91	2003 Apr 23	
12035812+0015500	20433	SDSS J120358.19+001550.3	L3	12.48	15.81	1.34E-11	> -10.85	7
1213033–043243	11044	...	L5	13	16.35	8.15E-12	> -2.52	2002 Jan 24	
12212770+0257198	20444	...	L0	11.95	15.16	2.43E-11	-5.96	3.66E-16	-4.82	2003 Apr 21	
1224522–123835	11068	BR 1222–1221	M9	11.37	14.52	4.38E-11	-7.14	7.29E-16	-4.78	2003 Apr 22	

TABLE 2—*Continued*

2MASS Designation	UCD #	Other Name	ST	K	M_{bol}	F_{bol}	H α EW (Å)	H α Flux	$\log(F_{H\alpha}/F_{bol})$	UT date	Spectra Ref
1246517+314811	11095	LHS 2632	M7.5	11.23	14.31	5.33E-11	> -0.12	8
1253124+403403	11109	LHS 2645	M7.5	11.17	14.25	5.63E-11	-5.76	6.40E-16	-4.94	2003 Jul 10	
1300425+191235	11115	...	L1	11.61	14.86	3.19E-11	> -0.40	2004 Feb 12	
1305401-254106 ^a	11122	Kelu-1	L2:	11.73	15.03	2.74E-11	-0.83	8.66E-17	-5.50	...	
1309218-233035	11127	CE 303	M8	10.67	13.76	8.80E-11	-5.12	3.32E-15	-4.42	2002 Jan 25	
1332244-044112	11153	...	M7.5	11.3	14.37	5.03E-11	-13.35	3.30E-15	-4.18	2002 Jan 27	
1356414+434258	11177	LP 220- 13	M7	10.63	13.69	9.42E-11	-16.52	7.39E-15	-4.11	2002 Jan 24	
1403223+300754	11188	...	M8.5	11.63	14.75	3.55E-11	-4.81	6.67E-16	-4.73	2003 Jul 10	
1411213-211950	11194	...	M9	11.32	14.47	4.59E-11	-5.98	3.63E-15	-4.10	2002 Jan 23	
14213145+1827407	20562	...	L0	11.94	15.15	2.46E-11	-2.04	5.90E-16	-4.62	2004 Feb 12	
14252798-3650229	20568	DENIS-P J142527.97-36502	L3	11.81	15.14	2.48E-11	> -5.71	2003 Apr 22	
14283132+5923354	20570	...	L5	13.27	16.61	6.40E-12	2005 Mar 5	
14284323+3310391	20571	LHS 2924/ LP 271-25/ GJ	M9	10.74	13.89	7.81E-11	-4.76	2.25E-15	-4.54	2003 Mar 14	
1438082+640836	11224	...	M9.5	11.57	14.75	3.55E-11	-2.36	1.81E-16	-5.29	2001 Jul 21	
14392836+1929149	20581	...	L1	11.55	14.80	3.37E-11	> -1.36	2003 Apr 22	
1440229+133923	11230	LSPM J1440+1339	M8	11.29	14.39	4.95E-11	-4.11	1.16E-15	-4.63	2002 Jul 5	
14482563+1031590	20587	...	L5	12.68	16.03	1.09E-11	> -8.33	2003 Apr 20	
1456383-280947	11264	LHS 3003	M7	8.92	11.97	4.58E-10	-7.58	1.43E-14	-4.51	2003 Mar 13	
15010818+2250020	20596	TVLM 513-46546	M9	10.71	13.85	8.09E-11	> -6.47	2003 Jul 10	
1506544+132106	11291	...	L3	11.75	15.08	2.61E-11	> -7.87	
1507277-200043	11294	...	M7.5	10.65	13.73	9.09E-11	-2.15	1.01E-15	-4.96	2002 Jan 27	
1507476-162738	11296	...	L5	11.3	14.65	3.90E-11	> -5.01	2004 Aug 9	
15101685-0241078	20602	TVLM 868-110639	M9	11.35	14.50	4.48E-11	> -5.82	2003 Mar 13	
15104786-2818174	20604	...	M9	11.69	14.84	3.28E-11	> -12.51	2003 Mar 13	
1515009+484739	11314	...	L6	12.57	15.88	1.25E-11	> -10.11	2004 Feb 10	
1521010+505323	11323	...	M7.5	10.92	14.00	7.10E-11	-8.52	9.49E-16	-4.87	2001 Jul 20	
1534570-141848	11346	...	M7	10.31	13.37	1.27E-10	-24.69	9.60E-15	-4.12	2002 Jul 4	
15394189-0520428	20625	DENIS-P J153941.96-05204	L3.5	12.58	15.92	1.21E-11	> -2.77	2004 Feb 10	
15394442+7437273	20626	...	M9	11.73	14.88	3.14E-11	> -5.22	2003 Mar 13	
1546054+374946	11439	...	M7.5	11.42	14.49	4.49E-11	-7.45	1.88E-15	-4.38	2003 Jul 10	
16073123-0442091	20660	...	M8	10.72	13.81	8.40E-11	-10.41	4.31E-15	-4.29	2003 Mar 14	
16154245+0546400	20662	...	M9	11.74	14.89	3.12E-11	> -2.58	2003 Apr 21	
1658037+702701	11668	...	L1	11.92	15.18	2.39E-11	> -13.55	2003 Mar 13	
17071830+6439331	20700	...	M9	11.38	14.52	4.37E-11	-28.74	2.58E-15	-4.23	2003 Jul 9	
17072343-0558249 ^a	20701	...	L0:	10.71	13.92	7.64E-11	> -3.43	2003 Apr 23	
1721039+334415	11694	...	L3	12.47	15.81	1.34E-11	> -1.89	2001 Jul 19	
17312974+2721233	20744	...	L0	10.91	14.12	6.34E-11	-5.98	8.92E-16	-4.85	2003 Apr 22	
17351296+2634475 ^a	20746	LSPM J1735+2634	M7.5:	10.16	13.23	1.44E-10	-2.60	1.08E-15	-5.13	2003 Apr 22	
17534518-6559559	20760	...	L4	12.42	15.77	1.38E-11	> 26.65	2003 Apr 23	
1757154+704201	11735	LP 44-162	M7.5	10.37	13.45	1.18E-10	-0.91	4.19E-16	-5.45	2003 Mar 13	
1807159+501531	11756	...	L1.5	11.61	14.89	3.12E-11	-1.38	8.49E-17	-5.57	2001 Jul 15	
1835379+325954	11792	LSR J1835+3259	M8.5	9.15	12.28	3.46E-10	-1.99	7.13E-16	-5.69	2001 Jul 22	
1843221+404021	11800	LHS 3406	M8	10.27	13.37	1.27E-10	-7.45	6.08E-15	-4.32	...	
18451889+3853248	20793	LSPM J1845+3853	M8	11.05	14.14	6.20E-11	-15.42	1.82E-15	-4.53	2003 Jul 9	
19360187-5502322	20823	SIPS 1936-5502	L4:	13.05	16.39	7.79E-12	> -7.77	2003 Apr 20	

TABLE 2—*Continued*

2MASS Designation	UCD #	Other Name	ST	K	M_{bol}	F_{bol}	H α EW (Å)	H α Flux	$\log(F_{H\alpha}/F_{bol})$	UT date	Spectra Ref
20004841–7523070	20845	...	M9	11.51	14.66	3.85E-11	> -6.87	2003 Apr 23	
20282035+0052265	20866	SDSS J202820.32+005226.5	L3	12.79	16.13	9.97E-12	> -6.33	2003 Jul 10	
20360316+1051295	20870	...	L3	12.45	15.78	1.37E-11	> -6.34	2003 Jul 9	
2037071–113756	12027	...	M8	11.26	14.36	5.09E-11	-6.23	1.70E-15	-4.48	2001 Jul 14	
20450238–6332066	20875	...	M9	11.21	14.36	5.10E-11	> -4.62	2003 Apr 20	
2057540–025230	12054	...	L1.5	11.75	15.03	2.74E-11	-8.44	4.01E-16	-4.83	2001 Jul 15	
2104149–103736	12059	...	L2.5	12.36	15.68	1.51E-11	> -3.41	2001 Jul 15	
2224438–015852	12128	...	L4.5	12.02	15.37	2.01E-11	-1.23	1.45E-17	-6.14	1999 Jul 16	
22264440–7503425	20946	DENIS-P J222644.3–750342	M8	11.25	14.34	5.16E-11	-3.15	3.81E-16	-5.13	2004 Aug 8	
2237325+392239	12145	G 216-7B	M9.5	12.15	15.33	2.08E-11	-0.7	2002 Jan 1	9
22521073–1730134 ^b	20976	DENIS-P J225210.73–17301	L5.5	12.9	16.23	9.04E-12	> 173.7	2005 Oct 9	
22551861–5713056	20979	...	L3	12.58	15.91	1.21E-11	> -20.33	2004 Aug 9	
2306292–050227	12171	...	M8	10.29	13.38	1.25E-10	-2.77	3.57E-16	-5.54	2003 Jul 10	
2325453+425148	13227	...	L8	13.81	17.01	4.44E-12	> -1.39	2004 Sep 20	
23464599+1129094	21011	LSPM J2346+1129	M9	11.61	14.75	3.53E-11	-13.01	1.15E-15	-4.49	2003 Jul 10	
2349489+122438	12217	LP 523–55	M8	11.56	14.66	3.86E-11	-2.33	4.46E-15	-3.94	2003 Jul 11	
2351504–253736	12220	...	M8	11.29	14.52	4.38E-11	> -2.80	2002 Jul 5	

a

NOTE.—Spectra references are only given when the data used to measure H α was not taken as part of the 2MASS sample spectral typing.

^aBinary considered as a single object due to the lack of resolved spectroscopy.

^bWide binary

References. — (1) Leinert, priv. comm. (2) Hawley et al. 2002 (3) Kirkpatrick, priv. comm. (4) Kirkpatrick et al. 1999 (5) Kirkpatrick et al. 1997 (6) Kirkpatrick et al. in prep (7) Fan et al. 2000 (8) Kirkpatrick et al. 1995 (9) Kirkpatrick et al. 2000

TABLE 3
H α EW FOR VARIABLE OBJECTS

2MASS Designation	Other Name	2MUPM Sample	Spectral Type	H α EW (Å)	UT Date	Reference
01090150–5100494	...	yes	M9	-114	2003 Nov 9	
				-31	2004 Aug 9	
0144353–071614	...	yes	L5	-24	2001 Feb 20	1
				>-3	2002 Jan 24	
0320596+185423	LP 412–31	yes	M8	-29	1995 Oct 28	2
				-29	1998 Dec	3
				-24	2000 Oct 1	
				-330	2002 Jan 23	
				-18	...	4
				-83	...	5
0853362–032932	LHS 2065	yes	M9	-261	1998 Dec 12	6
				-8	2003 Mar 14	
				-17	2003 Apr 21	
				-38	2002 Jan 23	
1016347+275149	LHS 2243	yes	M8	-1.3	1993 Jan 21	7
				-44	1998 Dec	3
				-7	2003 Jun 11	
10224821+5825453	...	yes	L1	-128	2004 Feb 10	
				-24	2004 Feb 11	
				-26	2004 Feb 12	
1028404–143843	...	no	M7	-23	2003 Apr 19	
				-12	2003 Apr 21	
				-14	2003 Apr 22	
				-71	2002 Jan 25	
1108307+683017	...	yes	L0.5	-8	1999 Jun	3
				>-1	2004 Mar 3	
1121492–131308	LHS 2397a	yes	M8	-12	1998 Dec	8
				-78	2002 Jan 23	
1224522–123835	BR 1222–1221	yes	M9	-7	2003 Jun 4	
				-23		4
1336406+374323	...	no	L1	-17	2002 Jul 22 (19:42)	
				>-5	2002 Jul 22 (20:58)	
13384944+0437315		no	L1	-11	2004 Feb 11	
				-28	2003 Apr 20	
1403223+300754	...	yes	M8.5	-19	1999 Jun	3
				-5	2003 Jul 30	
17071830+6439331	...	yes	M9	-29	2003 Jul 7	

References. — (1) Liebert et al. (2003) (2) Martín et al. (1996) (3) Gizis et al. (2000) (4) Reid et al. (2002) (5) Basri (2001) (6) Martín & Ardila (2001) (7) Martín et al. (1994) (8) Martín et al. (1999)

TABLE 4
LINE STRENGTHS FOR 2M 1028–14

Ion	λ (Å)	Continuum ^a	Line Flux ^a	EW (Å)
Ba II	6497	78	58	-0.736
H α	6563	80	7745	-96.66
He I	6678	75	265	-3.535
He I	7067	74	158	-2.146
He I	7281	72	28	-0.394
O I	7777	66	180	-2.727
Ca II	8498	67	404	-6.019
Ca II	8542	68	548	-8.124
Ca II	8662	72	409	-5.654
H(P11)	8863	72	100	-1.395
H(P10)	9015	69	178	-2.586
H(P9)	9230	80	204	-2.55
H(P8)	9546	63	340	-5.338

^ain units of 10^{-16} *ergs cm*⁻² *s*⁻¹